Journal of Virology

Effects of Aging on Influenza Virus Infection Dynamics

Esteban A. Hernandez-Vargas, Esther Wilk, Laetitia Canini, Franklin R. Toapanta, Sebastian C. Binder, Alexey Uvarovskii, Ted M. Ross, Carlos A. Guzmán, Alan S. Perelson and Michael Meyer-Hermann

J. Virol. **2014, 88(8):4123. DOI: 10.1128/JVI.03644-13.**
Published Ahead of Print 29 January 2014.

Updated information and services can be found at:
http://jvi.asm.org/content/88/8/4123

These include:

SUPPLEMENTAL MATERIAL Supplemental material

REFERENCES This article cites 60 articles, 16 of which can be accessed free at: http://jvi.asm.org/content/88/8/4123#ref-list-1

CONTENT ALERTS Receive: RSS Feeds, eTOCs, free email alerts (when new articles cite this article), more»

Information about commercial reprint orders: **http://journals.asm.org/site/misc/reprints.xhtml**
To subscribe to to another ASM Journal go to: **http://journals.asm.org/site/subscriptions/**

Journals.ASM.org

Downloaded from http://jvi.asm.org/ on March 31, 2014 by Helmholtz-Zentrum fuer Infektionsforschung - BIBLIOTHEK-

JVI Journals.ASM.org

Effects of Aging on Influenza Virus Infection Dynamics

Esteban A. Hernandez-Vargas,[a] Esther Wilk,[c] Laetitia Canini,[b] Franklin R. Toapanta,[d] Sebastian C. Binder,[a] Alexey Uvarovskii,[a] Ted M. Ross,[e] Carlos A. Guzmán,[f] Alan S. Perelson,[b] Michael Meyer-Hermann[a,g]

Department of Systems Immunology and Braunschweig Integrated Centre of Systems Biology, Helmholtz Centre for Infection Research, Braunschweig, Germany[a]; Theoretical Biology and Biophysics, Los Alamos National Laboratory, Los Alamos, New Mexico, USA[b]; Department of Infection Genetics, Helmholtz Centre for Infection Research, Braunschweig, Germany[c]; Center for Vaccine Development, University of Maryland, Baltimore, Maryland, USA[d]; Center for Vaccine Research, University of Pittsburgh, Pittsburgh, Pennsylvania, USA[e]; Department of Vaccinology and Applied Microbiology, Helmholtz Centre for Infection Research, Braunschweig, Germany[f]; Institute for Biochemistry, Biotechnology and Bioinformatics, Technische Universität Braunschweig, Braunschweig, Germany[g]

ABSTRACT

The consequences of influenza virus infection are generally more severe in individuals over 65 years of age (the elderly). Immunosenescence enhances the susceptibility to viral infections and renders vaccination less effective. Understanding age-related changes in the immune system is crucial in order to design prophylactic and immunomodulatory strategies to reduce morbidity and mortality in the elderly. Here, we propose different mathematical models to provide a quantitative understanding of the immune strategies in the course of influenza virus infection using experimental data from young and aged mice. Simulation results suggested a central role of $CD8^+$ T cells for adequate viral clearance kinetics in young and aged mice. Adding the removal of infected cells by natural killer cells did not improve the model fit in either young or aged animals. We separately examined the infection-resistant state of cells promoted by the cytokines alpha/beta interferon (IFN-α/β), IFN-γ, and tumor necrosis factor alpha (TNF-α). The combination of activated $CD8^+$ T cells with any of the cytokines provided the best fits in young and aged animals. During the first 3 days after infection, the basic reproductive number for aged mice was 1.5-fold lower than that for young mice ($P < 0.05$).

IMPORTANCE

The fits of our models to the experimental data suggest that the increased levels of IFN-α/β, IFN-γ, and TNF-α (the "inflammaging" state) promote slower viral growth in aged mice, which consequently limits the stimulation of immune cells and contributes to the reported impaired responses in the elderly. A quantitative understanding of influenza virus pathogenesis and its shift in the elderly is the key contribution of this work.

The recent outbreaks of H1N1 (swine flu), H5N1 (bird flu), and H7N9 virus infections have underlined the impact of influenza A virus infections and have shown that influenza A virus is a major threat for human health. The high degree of variability of the influenza virus due to reassortments and mutations (genetic shift and drift, respectively) is responsible for the continuous risk of epidemics and pandemics. Seasonal influenza virus infections account for annual hospitalization of 226,000 individuals in the United States (1). Typically, influenza virus infection involves the upper respiratory tract and the upper divisions of bronchi. In severe cases, the infection can spread to the alveolar region (2). Depending on the pathogenicity of the virus and the susceptibility of the host, other complications can also be observed (3–6), such as neurological symptoms caused by dissemination of the virus to the brain.

One important risk factor for influenza virus infections is age (7, 8). Currently, in industrialized countries, the majority of deaths associated with influenza virus infections occur in people over 65 years of age (1, 9). The immune system in the elderly is less efficient than that in younger people, and vaccination performs poorly (10). Immunosenescence is the decline of immune functions due to natural age progression. While recall responses to previously encountered antigens might be conserved, the ability to initiate a primary immune response against novel antigens decreases with age (11). The mechanisms leading to age-dependent alterations of the immune response are still not well understood (12).

Various age-related defects have been associated with the T cell compartment (13–15). Additionally, an increase in the basal levels of various inflammatory cytokines (e.g., macrophage inflammatory protein 1β [MIP-1β], tumor necrosis factor alpha [TNF-α], gamma interferon [IFN-γ], interleukin-1β [IL-1β], IL-6) has consistently been described in the elderly, a state dubbed "inflammaging" (16, 17). Humoral responses are also affected in seniors, with a decrease in the quantity of antibodies produced, alterations in the proportions of naive and memory B cell subsets, and decreased affinity-antibody maturation (18, 19).

Both the adaptive immune system and the innate response are altered during viral infections in the elderly (11, 20, 21). Experimental studies (22) have demonstrated that dendritic cells (DCs), the main antigen-presenting cells (APCs), from aged individuals have a reduced antigen-capture capacity, impaired migration, and a reduced T cell activation capacity. Further murine studies have

Received 18 December 2013 **Accepted** 19 January 2014

Published ahead of print 29 January 2014

Editor: A. García-Sastre

Address correspondence to Alan S. Perelson, asp@lanl.gov, or Michael Meyer-Hermann, mmh@theoretical-biology.de.

Supplemental material for this article may be found at http://dx.doi.org/10.1128/JVI.03644-13.

Copyright © 2014, American Society for Microbiology. All Rights Reserved.

doi:10.1128/JVI.03644-13

Downloaded from http://jvi.asm.org/ on March 31, 2014 by Helmholtz-Zentrum fuer Infektionsforschung - BIBLIOTHEK

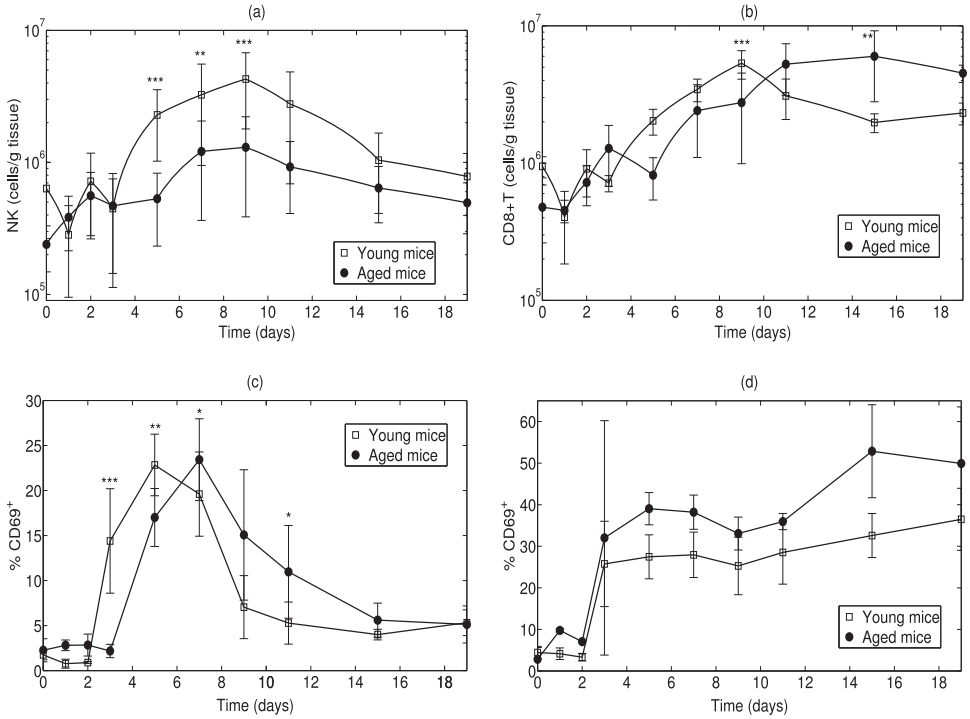

FIG 1 NK cell and $CD8^+$ T cell levels. (a) NK cell infiltration in the lungs of young and aged mice; (b) $CD8^+$ T cell infiltration in the lungs of young and aged mice; (c) percentage of activated NK cells ($CD3^-$, $CD19^-$, and $DX5^+$) determined by the expression of the activation marker $CD69^+$; (d) percentage of activated $CD8^+$ T cells ($CD3^+$, $CD4^-$, and $CD8^+$) determined by the expression of the activation marker $CD69^+$. Asterisks indicate statistically significant differences between aged and young animals: *, $P < 0.05$; **, $P < 0.01$; ***, $P < 0.001$. Data are reproduced from reference 24.

revealed that natural killer (NK) cells from the lungs of old mice have decreased IFN-γ production during influenza virus infection (23, 24).

Quantitative analyses of immune components and their respective interactions during influenza virus infection are crucial to develop prophylactic and therapeutic strategies to reduce morbidity and mortality. Thus, mathematical modeling has been used to capture the dynamics of influenza virus infection and to understand the interaction of the virus with the immune system (25–38). Much of the work has been focused on the basic relationship between the host and the virus (25, 26, 32, 34, 35), whereas other work has strived to quantify the interplay between viral replication and adaptive immunity (27–30, 36). These models have been important to estimate the kinetic parameters describing influenza virus infection (25, 26, 28–30, 35, 36).

Only a few influenza virus infection models have studied the innate immune response. For instance, models validated with equine data (29, 35, 36) have shown the importance of the kinetics of type I interferons (IFN-Is) in influenza virus pathology. Additionally, a model incorporating the killing of infected cells mediated by IFN-I-activated cells was suggested (36). Estimations of illness parameters and symptoms have also been introduced (34). Despite the large amount of activity in the modeling community, none of the prior modeling studies have examined age-related changes and their effects on influenza virus infection dynamics, which are the key aspects addressed in this work.

MATERIALS AND METHODS

Experimental data. The mouse model has proven to be invaluable in exploring the pathogenesis of influenza virus infection (39). Here, we consider the murine data presented elsewhere (24). Mice were infected with influenza virus A/Puerto Rico/8/34 (H1N1) at 12 to 16 weeks of age (young mice) or 72 to 76 weeks of age (aged mice). Lung virus titers were determined by plaque assay and reported as PFU per ml. The materials and methods are described in detail in reference 24. Animals were treated according to the guidelines of the Institutional Animal Care and Use Committee (IACUC) of the University of Pittsburgh. All the protocols used were approved by the IACUC of the University of Pittsburgh as previously described in reference 24. In short, mice were anesthetized and intranasally instilled with 50 to 100 PFU. Following infection, mice were monitored daily for morbidity and mortality. Lungs were harvested on days 0, 1, 2, 3, 5, 7, 9, 11, 15, and 19 postinfection.

Lungs were homogenized, and the supernatants were used to determine virus titers, immune cell populations, and cytokine and chemokine concentrations. Virus titers were determined using a multiplex bead array assay (Luminex, Austin, TX, USA) and reported as the numbers of PFU per ml.

In our model, we considered NK cells and $CD8^+$ T cells infiltrating the lungs of young and aged mice (Fig. 1a and b). NK cell and $CD8^+$ T cell activation were determined by use of the early activation marker CD69 (Fig. 1c and d).

In addition, we also considered the effects of different cytokines in our models: IFN-α (Fig. 2a), IFN-β (Fig. 2b), IFN-γ (Fig. 2c), and TNF-α (Fig. 2d). IFN-γ and TNF-α were determined using a multiplex bead array assay (Luminex, Austin, TX, USA). Meanwhile, IFN-α and IFN-β were determined by enzyme-linked immunosorbent assay, and these results have not been previously published.

Mathematical model. We used mathematical models based on ordinary differential equations (ODEs) to reveal the key age-related changes of the immune system between young and aged mice. To this end, we considered different immune strategies during influenza virus infection for both young and aged mice (Fig. 3).

Downloaded from http://jvi.asm.org/ on March 31, 2014 by Helmholtz-Zentrum fuer Infektionsforschung - BIBLIOTHEK-

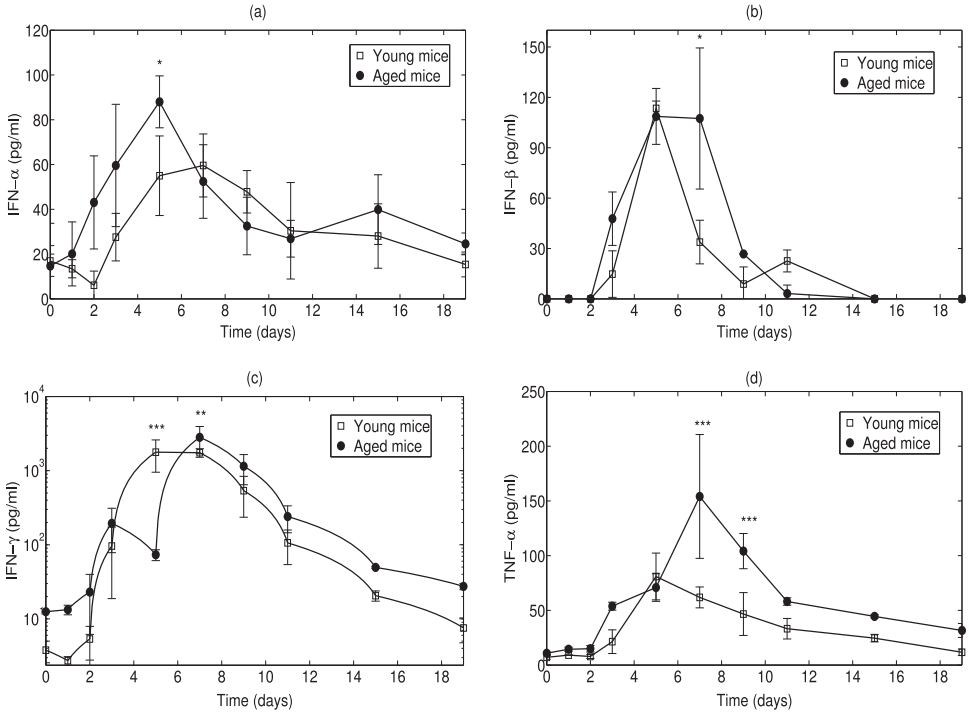

FIG 2 Cytokine levels in the supernatants of lung homogenates. The time course of IFN-α (a), IFN-β (b), IFN-γ (c), and TNF-α (d) concentrations is shown. Asterisks indicate statistically significant differences between aged and young animals: *, $P < 0.05$; **, $P < 0.01$; ***, $P < 0.001$. Data for IFN-γ and TNF are reproduced from reference 24. Data for IFN-α and IFN-β are newly unpublished.

The proposed models consider epithelial cells in the respiratory compartment. Cells can be in one of three possible states: susceptible (U), infected (I), or refractory (R). Virus (V) infects susceptible cells with rate constant β. Once cells are productively infected, they release virus at rate p. Virus particles are cleared at rate c.

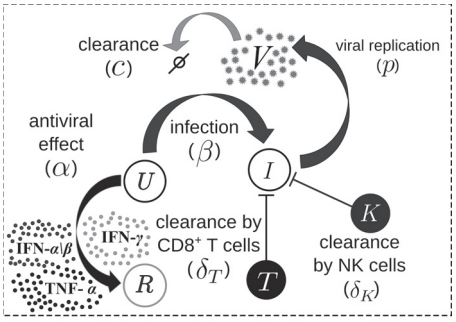

$$\frac{dU}{dt} = -\beta UV - \alpha U(F_\alpha + F_\beta + F_\gamma + F_{TNF})$$
$$\frac{dI}{dt} = \beta UV - \delta_T IT - \delta_K IK$$
$$\frac{dR}{dt} = \alpha U(F_\alpha + F_\beta + F_\gamma + F_{TNF})$$
$$\frac{dV}{dt} = pI - cV$$

FIG 3 Schematic representation of the influenza virus infection model and immune strategies. Epithelial cells are considered in one of the following states: susceptible (U), infected (I), and refractory (R). Infected cells produce virus particles (V) that infect other susceptible cells. Activated CD8$^+$ T cells (T) and activated NK cells (K) kill infected cells. IFN-α (F_α), IFN-β (F_β), IFN-γ (F_γ), and TNF-α (F_{TNF}) can promote the state of resistance to infection in epithelial cells.

CD8$^+$ T cells play a crucial role in the clearance of influenza virus infection (40). We included activated CD8$^+$ T cells (T) at time t [$T(t)$], which can kill infected cells at rate $\delta_T I(t)T(t)$. In addition, we also included the killing of infected cells by activated NK cells [$K(t)$], which occurs at rate $\delta_K I(t)K(t)$. We used the experimental data shown in Fig. 1 to model CD8$^+$ T cell and NK cell dynamics. Using piecewise linear fits for both young and aged mice, we generated a time-dependent function, $T(t)$, which represents the number of activated CD8$^+$ T cells, and $K(t)$, which represents the number of activated NK cells during influenza virus infection. The numbers of activated CD8$^+$ T and NK cells in the lung were computed by multiplying the total number of cells in Fig. 1a and b by the percentage of activated cells shown in Fig. 1c and d, respectively.

The release of IFN-Is is part of the innate immune response to viral infections. In this work, we considered the effects at time t of IFN-α [$F_\alpha(t)$], IFN-β [$F_\beta(t)$], IFN-γ [$F_\gamma(t)$], and TNF-α [$F_{TNF}(t)$]. The rate at which different cytokines induce the antiviral state in susceptible cells is represented by $\alpha U[F_\alpha(t) + F_\beta(t) + F_\gamma(t) + F_{TNF}(t)]$, where α is a constant. $F_\alpha(t)$, $F_\beta(t)$, $F_\gamma(t)$, and $F_{TNF}(t)$ are piecewise linear functions derived by fitting the data shown in Fig. 2.

Initial conditions. For initial conditions, the number of epithelial cells (U_0) is taken as 10^7 cells (24). Initial values for infected (I_0) and refractory (R_0) cells are considered 0. V_0 is constrained to be at levels below detectable levels (less than 50 PFU/ml). Previous work has suggested using half of the detection levels (41); thus, we consider V_0 to be 25 PFU/ml.

Parameter estimation. Parameter fitting was performed by minimizing the root mean square (RMS) difference on a log scale between the model predictive output ($\bar{y}_i$) and the experimental measurement (y_i) as follows:

$$\text{RMS} = \sqrt{\frac{1}{n}\sum_{i=1}^{n}[\log(y_i) - \log(\bar{y}_i)]^2} \quad (1)$$

where i is the corresponding sample and n is the total number of measurements. Differential equations were solved in MATLAB using the solver

Downloaded from http://jvi.asm.org/ on March 31, 2014 by Helmholtz-Zentrum fuer Infektionsforschung - BIBLIOTHEK-

TABLE 1 Model comparison using different immune strategies[a]

Model no.	Model	Fit	Young mice		Aged mice	
			RMS	AIC_c	RMS	AIC_c
M1	$\dot{U} = -\beta UV, \dot{I} = \beta UV - \delta I, \dot{V} = pI - cV$	β, δ	1.48	50.65	1.59	62.51
M2	$\dot{U} = -\beta UV, \dot{I} = \beta UV - \delta_T IT, \dot{V} = pI - cV$	β, δ_T	1.25	30.60	1.58	57.43
M3	$\dot{U} = -\beta UV, \dot{I} = \beta UV - \delta_T IT - \delta_K IK, \dot{V} = pI - cV$	$\beta, \delta_T, \delta_K$	1.25	32.64	1.58	62.94
M4	$\dot{U} = -\beta UV, \dot{I} = \beta UV - \delta_K IK, \dot{V} = pI - cV$	β, δ_K	1.38	42.47	1.70	72.54
M5	$\dot{U} = -\beta UV - \alpha U(F_\alpha + F_\beta), \dot{I} = \beta UV - \delta_T IT, \dot{V} = pI - cV, \dot{R} = \alpha U(F_\alpha + F_\beta)$	β, δ_T, α	1.22	28.94	1.36	44.27
M6	$\dot{U} = -\beta UV - \alpha U F_\gamma, \dot{I} = \beta UV - \delta_T IT, \dot{V} = pI - cV, \dot{R} = \alpha U F_\gamma$	β, δ_T, α	1.23	30.58	**1.35**	**43.27**
M7	$\dot{U} = -\beta UV - \alpha U F_{TNF}, \dot{I} = \beta UV - \delta_T IT, \dot{V} = pI - cV, \dot{R} = \alpha U F_{TNF}$	β, δ_T, α	**1.21**	**28.34**	1.36	44.01
M8	$\dot{U} = -\beta UV - \alpha U(F_\alpha + F_\beta + F_\gamma + F_{TNF}), \dot{I} = \beta UV - \delta_T IT, \dot{V} = pI - cV, \dot{R} = \alpha U(F_\alpha + F_\beta + F_\gamma + F_{TNF})$	β, δ_T, α	1.22	29.78	1.36	43.74

[a] The best-fitting, minimum values for RMS and AIC_c in a comparison of all models are in bold. Further descriptions of parameter values can be found in Tables SA.1 to SA.7 in the supplemental material.

ode45. The minimization of RMS was performed using the differential evolution (DE) algorithm (42). We tried several optimization solvers, including both deterministic methods (fmincon MATLAB routine, threshold acceptance algorithm, and pattern search algorithm) and stochastic methods (genetic algorithm and annealing algorithm). We observed that the DE global optimization algorithm is robust to initial guesses of parameters and converges faster with more certainty than the other methods mentioned.

Confidence interval. The 95% confidence intervals of the parameter estimates were computed using the bootstrap method (43), implemented as follows: we generated for each time point a vector with random numbers using a distribution with the mean and variance corresponding to the experimental data. This was repeated 1,000 times. In each repetition, we refit our model to obtain the corresponding parameter distribution.

Statistics. Analysis of the experimental data for young and aged mice at different time points was implemented by two-way analysis of variance tests. Significance was identified as a P value of <0.05. The data were further analyzed by a two-way t test and a Bonferroni posttest.

AIC. The Akaike information criterion (AIC) is a way to compare the goodness of fit for different models. A lower AIC value means that the model describes the data better. For a small number of data points, the corrected AIC (AIC_c) has the following form:

$$AIC_c = n \log\left(\frac{RSS}{n}\right) + \frac{2mn}{n - m - 1} \quad (2)$$

where n is the number of data points, m is the number of unknown parameters, and RSS is the residual sum of squares obtained from the fitting routine (44).

Parameters to evaluate infectivity. Infectivity is the ability of a pathogen to establish an infection. To determine infectivity, we used the basic reproductive number (R_N), which is roughly defined as the expected number of secondary infections produced by an infected cell in its lifetime (45). For the model presented in Fig. 3, R_N is computed at different time points to evaluate the evolution of the infection, that is

$$R_N = \frac{U(t)p\beta}{c[\delta_T T(t) + \delta_K K(t)]} \quad (3)$$

Parameter identifiability and sensitivity. A system that is algebraically identifiable may still be practically nonidentifiable if the amount and quality of the data are insufficient and the data manifest large deviations. The novel approach shown elsewhere (46) exploits the profile likelihood to determine identifiability and is considered here. This approach is able to detect both structurally and practically nonidentifiable parameters. In addition, to explore practical identifiability and parameter sensitivity, we generated scatter plots of pairs of parameters over different bootstrap replicates. This provides visual evidence of how bounded the parameter distributions are and whether two parameters depend on one another such that their individual values cannot be independently determined.

RESULTS

The measurements presented previously (24) revealed a delay of about 1 day ($P < 0.05$) in the infiltration of $CD8^+$ T cells and NK cells into the lungs of aged mice compared to those of young mice (Fig. 1a and b). However, there was a statistically insignificant difference in the activation of these cells (Fig. 1c and d). Despite the delay in infiltration, influenza virus grew slower in aged animals than in young animals and reached a 10-fold lower peak viral load in aged animals than in young animals ($P < 0.05$).

The combined effect of innate and adaptive immune responses provides a difficult scenario to unravel the underlying mechanisms during influenza virus infection. Therefore, we propose different models in Table 1 to explore possible modes of action of the immune system.

Target cell limited model. The target cell limited model (M1) presented in Table 1 was originally proposed elsewhere (26). Previous work (26, 47) used model M1 because of its simplicity and ability to estimate parameters from viral titer data. The estimated model parameter values obtained by fitting model M1 to young and aged mouse data are given in Table SA.1 in the supplemental material. M1 provided worse fits (Fig. 4) than the other models shown in Table 1.

$CD8^+$ T cell response. Introducing a $CD8^+$ T cell response into model M1 led to model M2 (Table 1). In this model, we assumed that the clearance of infected cells is given by the term $\delta_T T(t) I(t)$, where $T(t)$ is the measured number of activated $CD8^+$ T cells in the lung (Fig. 1b and d) and δ_T is the killing rate by $CD8^+$ T cells. The respective best-fit model parameters are presented in Table SA.2 in the supplemental material. The use of the $CD8^+$ T cell response led to a model that fits the viral load data better, reducing AIC values with respect to those in model M1 (Table 1).

$CD8^+$ T cell and NK cell responses. The importance of NK cells during virus infection has been demonstrated by the increased susceptibility to viral infections of humans lacking NK cells (48). Similar results have been reported in mice (40). Thus, in order to examine the effect of NK cells on infected cell death, we added the term $\delta_K K(t) I(t)$, where $K(t)$ is the number of activated NK cells in the lung (Fig. 1a and c). This led to model M3 in Table 1.

The parameter δ_K is the rate constant for the killing of infected cells by NK cells (see Table SA.3 in the supplemental material). Fitting of model M3 (Table 1) to the data revealed that including killing of infected cells by NK cells does not improve the fits to the viral load data. The parameter δ_K for both young and aged mice

Downloaded from http://jvi.asm.org/ on March 31, 2014 by Helmholtz-Zentrum fuer Infektionsforschung - BIBLIOTHEK-

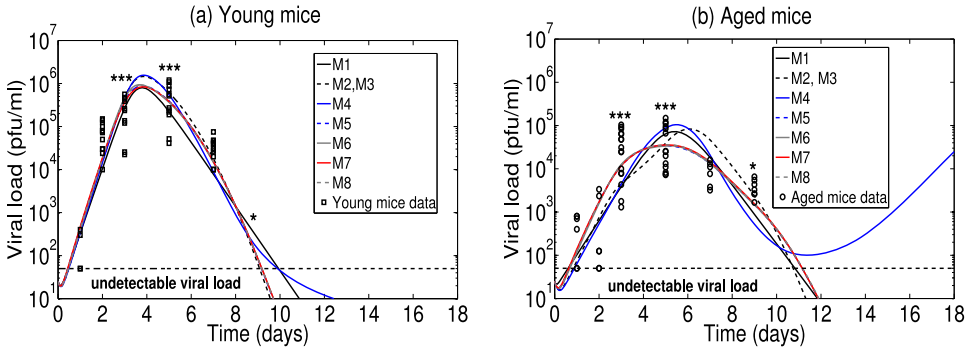

FIG 4 Model fitting for young and aged mice. Viral titer data from reference 24 and simulation results for young mice (a) and aged mice (b) are shown. Experimental results show that the viral titer was not detectable (less than 50 PFU/ml, shown with a horizontal dashed line) at day 9 for 6 young mice and at day 11 for 6 aged mice. Asterisks indicate statistically significant differences between aged and young animals: *, $P < 0.05$; ***, $P < 0.001$.

tended to very small values (10^{-8}), leading to the same dynamics as model M2 (Fig. 4).

To reveal if NK cells alone can provide better fits to the data than model M3, we removed from model M3 the $CD8^+$ T response, and this led to model M4. The trajectories in Fig. 4 show that the NK cell response ($\delta_K KI$) alone is not enough for viral clearance. Simulations suggested a possible rebound in the viral load of aged mice after day 11 postinfection, even though the killing capacity by NK cells (δ_K) was 3-fold larger than the killing capacity by $CD8^+$ T cells (δ_T) (see Table SA.4 in the supplemental material).

$CD8^+$ T cell and cytokines. Type I interferons (IFN-Is; IFN-α/β) and type II interferons (IFN-IIs; IFN-γ) possess key roles in determining the rate of virus replication in the initial stages of infection and in shaping the initial inflammatory and downstream adaptive immune responses (49, 50). In addition to type I and II interferons, previous experimental studies (51) revealed that TNF-α not only serves in the first line of defense against influenza virus infection but also has stronger antiviral activity against influenza virus than IFN-α/β or IFN-γ. The effect of cytokines is modeled by the use of piecewise linear functions of the data for IFN-α (F_α), IFN-β (F_β), IFN-γ (F_γ), and TNF-α (F_{TNF}) (Fig. 2).

The cytokine-induced antiviral effect on susceptible cells is represented by α. The algebraic identifiability study in Table SD.1 in the supplemental material reveals a second-order derivative ($\ddot{V}$) for all models, suggesting that a maximum of 3 parameters can be fitted because experimental data points were measured only 5 times (24). Therefore, we included $\alpha U(F_\alpha + F_\beta)$ in model M2 to generate model M5, αUF_γ in model M2 to generate model M6, $\alpha\ UF_{TNF}$ in model M2 to generate model M7, and $\alpha U(F_\alpha + F_\beta + F_\gamma + F_{TNF})$ in model M2 to generate model M8. Parameter values for model M5 are shown in Table SA.5 in the supplemental material, those for model M6 are shown in Table SA.6 in the supplemental material, those for model M7 are shown in Table 2, and those for model M8 are shown in Table SA.7 in the supplemental material. For both young and aged mice, all models with a cytokine-induced antiviral effect (models M5 to M8) provided very similar RMS and AIC values and better estimations than model M2 (Table 1).

Table 1 reveals that the best fits are achieved by the effects of TNF-α in young animals and by the effects of IFN-γ in aged animals. The effects of individual cytokines provide better fits than the effects of all cytokines combined in model M8. This suggests that each cytokine would promote different rates of acquisition of the resistant state in epithelial cells, that is, $U(\alpha_1 F_\alpha + \alpha_2 F_\beta + \alpha_3 F_\gamma + \alpha_4 F_{TNF})$. However, on the basis of only the viral load data, it is not possible to fit all cytokine parameters (α_1, α_2, α_3, and α_4).

Practical identifiability analysis based on the likelihood principle (46) revealed that the parameter p is difficult to identify due to the flat vertex in RMS parabolas for both young animals (see Fig. SE.1 in the supplemental material) and aged animals (see Fig. SE.2 in the supplemental material). Practical identifiability studies indicate that we can fix the values of p and c over a large range (p, from 0.1 to 7; c, from 3 to 10) without significantly altering RMS values. Structural and practical identifiability showed that parameter c is difficult but still possible to estimate due to the correlation with δ_T (see Fig. SE.3 and SE.4 in the supplemental material). We followed previous estimates of c equal to 4.2 day^{-1} for influenza virus infection in mice (30), and we fixed p equal to 1 PFU/ml · day^{-1}. Practical identifiability (see Fig. SE.5 and SE.6 in the supplemental material) also revealed that it is not possible to estimate a viral cytopathic effect (δI) when clearance by immune cells, for instance, $\delta_T TI$, is also included.

Bootstrap fits. Data presented elsewhere (24) showed that mice present a highly variable response to infection with influenza virus. To mimic a stochastic environment of the infection, we performed bootstrap fits for model M5 (see Fig. SB.1 to SB.6 in the supplemental material) and model M7 (see Fig. SC.1 to SC.4 in the supplemental material), and there were no significant differences in predictions and fits. Therefore, for the sake of clarity, we describe only the bootstrap fits for model M7, which is based on the $CD8^+$ T cell response and TNF-α.

For young and aged mice, the bootstrap fits in model M7 pre-

TABLE 2 Model parameters values in young and aged mice for model M7[a]

Mouse group	α (day^{-1} [10^{-3}])	δ_T ($cell^{-1}$ · day^{-1} [10^{-6}])	β (ml/PFU · day^{-1} [10^{-6}])
Young mice[b]	15.6 (0.10–23.31)	2.69 (2.40–2.96)	3.54 (2.85–4.65)
Aged mice[b]	15.3 (9.00–24.40)	1.43 (1.21–1.69)[c]	2.27 (1.83–2.91)[c]
Reference value range[d]	0.69–120 (36)	0.0001–50 (30)	0.11–190 (26, 30, 36)

[a] The following parameters were fixed for young and aged mice: $V_0 = 25$ PFU/ml, $p =$ 1 PFU/ml · day^{-1}, and $c = 4.2$ day^{-1}.
[b] The data in parentheses in these rows are 95% confidence intervals.
[c] Statistically significant difference ($P < 0.05$) between aged and young animals.
[d] The source(s) is given in parentheses.

Downloaded from http://jvi.asm.org/ on March 31, 2014 by Helmholtz-Zentrum fuer Infektionsforschung - BIBLIOTHEK-

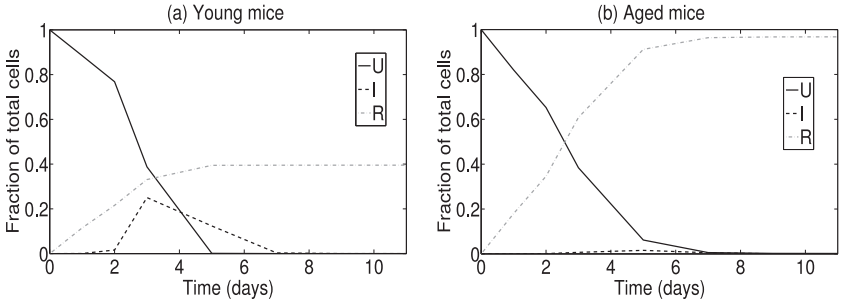

FIG 5 Cell fraction mean from bootstrap fits of model M7. Further details of the cell distribution can be found in Fig. SC.1 to SC.4 in the supplemental material.

dicted that the fraction of susceptible epithelial cells rapidly decreased (Fig. 5) to levels less than 50% of the initial values at 3 to 4 days postinfection (dpi). Cycles of cell infection resulted in an exponential growth of the viral titer, which peaked over time scales similar to those for infected cells. The predicted maximum fraction of infected cells in Fig. 5 is approximately 30-fold larger in young mice than in aged mice ($P < 0.05$). Cell distributions can be found in Fig. SC.1 to SC.3 in the supplemental material.

TNF-α, like other cytokines, may induce an antiviral state in epithelial cells (51), limiting the infection to other cells, which is modeled with the term αUF_{TNF}. TNF-α measurements in the supernatants of lung homogenates (Fig. 2d) showed that the average TNF-α concentration in aged mice was 2-fold higher than that in young mice at day 3. In addition, type I and II interferons in aged animals were present at levels higher than those in young mice (Fig. 2a to c).

Bootstrap fits in Fig. 5 show that while the virus is invading susceptible epithelial cells, TNF-α can coordinate an effective protective mechanism, increasing the number of refractory cells to levels 2-fold greater in aged animals than young animals ($P < 0.05$). A similar observation was obtained for type I interferons (see Fig. SB.1 to SB.6 in the supplemental material). Therefore, either the type I interferon, type II interferon, or TNF-α response can limit the exponential growth of viral titers. This suggests that the early limitation of viral growth at 3 to 4 dpi for both young and aged mice may be due to the decline of susceptible cells as they are converted to the refractory state, consistent with observations made previously (36).

Table 2 and Fig. 6 reveal important alterations in parameter values between young and aged mice and suggest that other differences may exist in the elderly. The main parameter changes found between young and aged mice are the following: the infection rate (β) was decreased by 30% ($P < 0.05$), and the rate of clearance of infected cells by $CD8^+$ T cells (δ_T) was decreased by 45% ($P < 0.05$). The TNF-α-induced antiviral effect on susceptible cells (α) did not present a significant difference in the elderly. These results are consistent with those for type I interferons (see Fig. SB.1 to SB.6 in the supplemental material).

The viral titer was measured as numbers of PFU/ml, because the measurements were performed in Madin-Darby canine kidney (MDCK) cells rather than murine lung cells; the parameters β and p, which are in units of PFU/ml, may not reflect *in vivo* rates. In addition, these two parameters are log-linearly correlated in young animals (see Fig. SE.1 in the supplemental material) and aged animals (see Fig. SE.2 in the supplemental material). Scatter plots from bootstrap fits in the form of two-parameter projections in Fig. 7 reveal that there are no strong correlations between β, α, and δ_T.

The combination of parameters that define the basic reproductive number can provide insights into age-related changes. Figure 8 demonstrates that the basic reproductive number (R_N) is statistically significantly ($P < 0.05$) larger in young animals than in aged animals during the first 3 dpi. Nevertheless, after 3 dpi, the basic reproductive number in aged animals is larger than that in young animals. This suggests that the slow growth of influenza virus in aged animals during the first 3 dpi is critical for the different infection processes in the elderly.

DISCUSSION

The mechanisms responsible for viral control during influenza virus infection remain subject to discussion. Whereas much research has been done on the pathogen, our understanding of the host response and the host-pathogen interaction, particularly with regard to the age of the host, is still very limited. Host-derived factors responsible for susceptibility or resistance to influenza A virus have been insufficiently investigated. One host parameter that has proven to be a risk factor for influenza virus infections and complications is age. Many hypotheses about how age affects

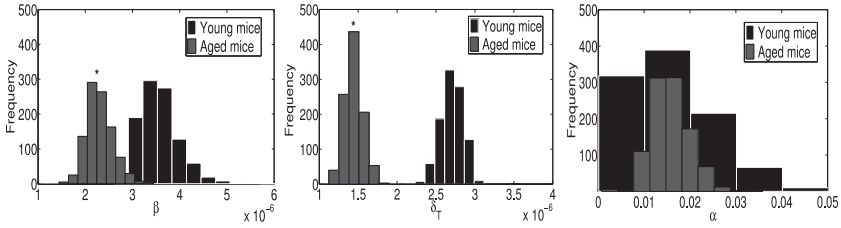

FIG 6 Parameter distribution from bootstrap fits of model M7. Asterisks indicate statistically significant differences between aged and young animals: *, $P < 0.05$.

Downloaded from http://jvi.asm.org/ on March 31, 2014 by Helmholtz-Zentrum fuer Infektionsforschung - BIBLIOTHEK-

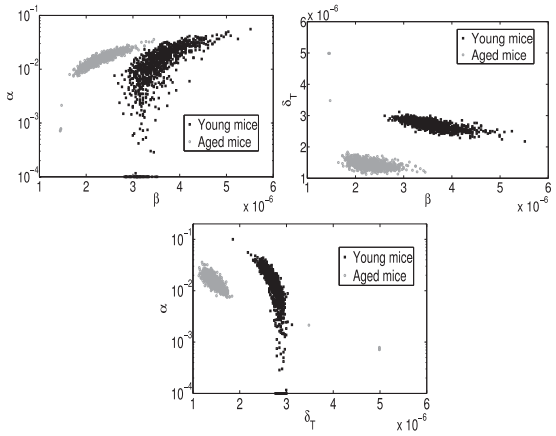

FIG 7 Parameter ensembles from bootstrap fit of model M7.

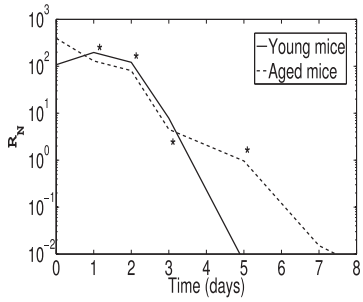

FIG 8 Mean basic reproductive number (R_N) from bootstrap fits of model M7. Further details of the distribution can be found in Fig. SC.4 in the supplemental material. Asterisks indicate statistically significant differences between aged and young animals: *, $P < 0.05$.

the immune system have been discussed in the literature (14, 52–54). The scenario becomes more complex in seniors, as vaccine efficacy is also affected by age. For influenza vaccines, an efficacy of 70 to 90% has been observed in young adults, while it is only 17 to 53% in the elderly (10, 55). In order to enhance vaccine efficacy in the elderly (56, 57), we need to better understand the immune responses to influenza virus infection and influenza vaccines. This study is a step forward in this direction.

The innate immune system is crucial to mediate early defense against viral infections (58). Type I and type II interferons are key players with relevant antiviral properties against influenza virus and shaping the downstream adaptive immune responses (49, 50). TNF-α has been suggested (51) to serve in the first line of defense against influenza virus infection, promoting stronger antiviral activity against influenza virus than IFN-α /β or IFN-γ.

Table 1 revealed that the use of IFN-I, IFN-II, or TNF-α data provides similar fits. Therefore, we presume that these three cytokines are redundant in mediating antiviral effects during influenza virus infection. However, these cytokines can shape the adaptive immune response in different ways, but such underlying mechanisms are not considered in our models.

Our models using IFN-I, IFN-II, or TNF-α are consistent with the results presented previously (36) that the early limitation of viral growth at 3 to 4 dpi can be explained by the decline of susceptible cells due to entry into the refractory state. In addition, Fig. 5 suggests that TNF-α may generate more refractory cells at 5 dpi in aged animals than in young animals ($P < 0.05$).

Experimental studies in mice deficient in B cells and T cells (59, 60) revealed that NK cells are able to control the virus similarly to wild-type mice for a certain time but do not prevent death due to the inability to eradicate the pathogen completely. Our results in Fig. 4 indicate that including the killing effect of NK cells does not improve the fit. This differs from the findings of previous results (34, 36); however, those studies did not include any NK data in the fitting. We presume that the main importance of NK cells is to promote the cytokines that limit the viral burden until $CD8^+$ T cells are primed and activated (48, 60).

The adaptive immune system is critical for the control and clearance of influenza virus infection (40). Experimental data for $CD8^+$ T cells in Fig. 1 show that this response starts at 3 dpi in young mice and increases log linearly, peaking at approximately 6×10^6 cells at day 9 dpi. Furthermore, experimental results reveal that the viral load is depleted to undetectable levels by the time that the $CD8^+$ T cells peak. In aged mice, there is a delay of approximately 5 days before any substantial increase in $CD8^+$ T cells ($P < 0.05$). The viral clearance occurs 1 to 2 days later in aged mice than in young mice ($P < 0.05$), which can be explained by the delay in the $CD8^+$ T cell response (Fig. 1).

Previous predictions (36) suggested that the adaptive immune response promotes the viral load to drop below detectable limits. However, the authors (36) modeled the adaptive immune response with a time-varying parameter, increasing the cell death rate or the viral clearance rate at a certain time. Of course, with appropriately selected time-varying parameters, the full course of the disease can be represented. Here, we considered a different approach and used the experimentally measured changes in activated $CD8^+$ T cells in the lung to represent the time-varying nature of the cell-mediated immune response to influenza virus.

Several studies (25, 26, 33, 34, 36), including ours, suggest that influenza virus grows rapidly in young hosts. However, we observed (Fig. 5) that the rate of infection of epithelial cells was significantly lower ($P < 0.05$) in aged mice than in young animals. This generated a more predominant viral load plateau in aged animals, leading to virus clearance at 11 dpi instead of 9 dpi for young mice (Fig. 4).

Examining the results presented in Fig. 8 and the experimental data in Fig. 1, we may formulate the following scenario for the impaired immune response to influenza virus infection in the elderly: the slower growth of influenza virus, with an R_N 1.5-fold smaller in aged animals than in young animals during the first 3 dpi ($P < 0.05$) and the 10-fold lower peak viral load ($P < 0.01$), leads to less immune stimulation. It has been established that a certain level of the pathogen and the resulting tissue damage are required to trigger immune activation (61), consistent with the observation that there is impaired stimulation of the immune system in the elderly (22, 62).

Thus, the reduced growth of influenza virus in aged mice may lead to limited activation of the acquired immune system, which ultimately leads to slow viral clearance. The reduced replication efficacy of the virus could be directly related to the large number of protected cells (R) in aged mice compared to the number in young ones promoted by either IFN-I, IFN-II, or TNF-α. Our results suggest that the inflammaging state (increase of basal levels of various inflammatory cytokines, e.g., MIP-1β, TNF-α, IFN-γ) described in the elderly (16, 17) is the key mechanism explaining the

Downloaded from http://jvi.asm.org/ on March 31, 2014 by Helmholtz-Zentrum fuer Infektionsforschung - BIBLIOTHEK

difference in the viral load between young and aged animals in this work.

Finally, it is worth mentioning that the data were generated from animals naive for influenza virus infection. In humans, the situation is more complicated by preexisting immunity against the virus as a result of either infection or vaccination in the past.

ACKNOWLEDGMENTS

This work was supported by the BMBF-GerontoSys initiative (GerontoShield), portfolio HGF (metabolic dysfunction), NIH grant OD011095, and NIH contract HHSN272201000055C (to A.S.P.). This work was performed in part while E. A. Hernandez-Vargas was a visitor at LANL with support from the International Network in Theoretical Immunology (PIRSESGA-2008-230665).

REFERENCES

1. **WHO.** 2011. Manual for the laboratory diagnosis and virological surveillance of influenza. Technical report. WHO, Geneva, Switzerland.
2. **Riel DV, Munster V, de Wit ED, Rimmelzwaan GF, Fouchier RA, Osterhaus AD, Kuiken T.** 2006. H5N1 virus attachment to lower respiratory tract. Science **312:**399. http://dx.doi.org/10.1126/science.1125548.
3. **de Jong MD, Bach VC, Phan TQ, Vo MH, Tran TT, Nguyen BH, Beld M, Le TP, Truong HK, Nguyen VVC, Tran TH, Do QH, Farrar J.** 2005. Fatal avian influenza A (H5N1) in a child presenting with diarrhea followed by coma. N. Engl. J. Med. **352:**686–691. http://dx.doi.org/10.1056/NEJMoa044307.
4. **Guleria R, Kumar J, Mohan A, Wig N.** 2009. Influenza A: from highly pathogenic H5N1 to pandemic 2009 H1N1. Epidemiology and clinical features. Indian J. Microbiol. **49:**315–319. http://dx.doi.org/10.1007/s12088-009-0056-3.
5. **Surana P, Tang S, McDougall M, Tong CYW, Menson E, Lim M.** 2011. Neurological complications of pandemic influenza A H1N1 2009 infection: European case series and review. Eur. J. Pediatr. **170:**1007–1015. http://dx.doi.org/10.1007/s00431-010-1392-3.
6. **CDC.** 2012. Severe influenza among children and young adults with neurologic and neurodevelopmental conditions—Ohio, 2011. MMWR Morb. Mortal. Wkly. Rep. **60:**1729–1733.
7. **Viboud C, Boelle P-Y, Cauchemez S, Lavenu A, Valleron AJ, Flahault A, Carrat F.** 2004. Risk factors of influenza transmission in households. Br. J. Gen. Pract. **54:**684–689. http://dx.doi.org/10.1016/j.ics.2004.01.013.
8. **Lee N, Shin MS, Kang I.** 2012. T-cell biology in aging, with a focus on lung disease. J. Gerontol. A Biol. Sci. Med. Sci. **67:**254–263. http://dx.doi.org/10.1093/gerona/glr237.
9. **Lemaitre M, Carrat F, Rey G, Miller M, Simonsen L, Viboud C.** 2012. Mortality burden of the 2009 A/H1N1 influenza pandemic in France: comparison to seasonal influenza and the A/H3N2 pandemic. PLoS One **7:**e45051. http://dx.doi.org/10.1371/journal.pone.0045051.
10. **Aspinall R, Del Giudice G, Effros RB, Grubeck-Loebenstein B, Sambhara S.** 2007. Challenges for vaccination in the elderly. Immun. Ageing **4:**9. http://dx.doi.org/10.1186/1742-4933-4-9.
11. **Ginaldi L, Loreto MF, Corsi MP, Modesti M, De Martinis M.** 2001. Immunosenescence and infectious diseases. Microbes Infect. **3:**851–857. http://dx.doi.org/10.1016/S1286-4579(01)01443-5.
12. **Nikolich-Zugich J.** 2012. The aging immune system: challenges for the 21st century. Immunology **24:**301–302. http://dx.doi.org/10.1016/j.smim.2012.09.001.
13. **Cambier J.** 2005. Immunosenescence: a problem of lymphopoieses, homeostasis, microenvironment, and signaling. Immunol. Rev. **205:**5–6. http://dx.doi.org/10.1111/j.0105-2896.2005.00276.x.
14. **Nikolich-Zugich J.** 2008. Ageing and life-long maintenance of T-cell subsets in the face of latent persistent infections. Nat. Rev. Immunol. **8:**512–522. http://dx.doi.org/10.1038/nri2318.
15. **Nikolich-Zugich J, Li G, Uhrlaub JL, Renkema KR, Smithey MJ.** 2012. Age-related changes in CD8+ T cell homeostasis and immunity to infection. Immunology **24:**356–364. http://dx.doi.org/10.1016/j.smim.2012.04.009.
16. **Le Saux S, Weyand CM, Goronzy JJ.** 2012. Mechanisms of immunosenescence: lessons from models of accelerated immune aging. Ann. N. Y. Acad. Sci. **1247:**69–82. http://dx.doi.org/10.1111/j.1749-6632.2011.06297.x.
17. **Cavanagh MM, Weyand CM, Goronzy JJ.** 2012. Chronic inflammation and aging: DNA damage tips the balance. Curr. Opin. Immunol. **24:**488–493. http://dx.doi.org/10.1016/j.coi.2012.04.003.
18. **Frasca D, Riley RL, Blomberg BB.** 2005. Humoral immune response and B-cell functions including immunoglobulin class switch are downregulated in aged mice and humans. Immunology **17:**378–384. http://dx.doi.org/10.1016/j.smim.2005.05.005.
19. **Ademokun A, Wu YC, Dunn-Walters D.** 2010. The ageing B cell population: composition and function. Biogerontology **11:**125–137. http://dx.doi.org/10.1007/s10522-009-9256-9.
20. **Leng J, Goldstein DR.** 2010. Impact of aging on viral infections. Microbes Infect. **12:**1120–1124. http://dx.doi.org/10.1016/j.micinf.2010.08.009.
21. **Solana R, Tarazona R, Gayoso I, Lesur O, Dupuis G, Fulop T.** 2012. Innate immunosenescence: effect of aging on cells and receptors of the innate immune system in humans. Immunology **24:**331–341. http://dx.doi.org/10.1016/j.smim.2012.04.008.
22. **Liu WM, van der Zeijst BAM, Boog CJ, Soethout EC.** 2011. Aging and impaired immunity to influenza viruses: implications for vaccine development. Hum. Vaccin. **7:**94–98. http://dx.doi.org/10.4161/hv.7.0.14568.
23. **Beli E, Clinthorne JF, Duriancik DM, Hwang I, Kim S, Gardner EM.** 2011. Natural killer cell function is altered during the primary response of aged mice to influenza infection. Mech. Ageing Dev. **132:**503–510. http://dx.doi.org/10.1016/j.mad.2011.08.005.
24. **Toapanta FR, Ross TM.** 2009. Impaired immune responses in the lungs of aged mice following influenza infection. Respir. Res. **10:**112. http://dx.doi.org/10.1186/1465-9921-10-112.
25. **Möhler L, Flockerzi D, Sann H, Reichl U.** 2005. Mathematical model of influenza A virus production in large-scale microcarrier culture. Biotech. Bioeng. **90:**46–58. http://dx.doi.org/10.1002/bit.20363.
26. **Baccam P, Beauchemin C, Macken CA, Hayden FG, Perelson AS.** 2006. Kinetics of influenza A virus infection in humans. J. Virol. **80:**7590–7599. http://dx.doi.org/10.1128/JVI.01623-05.
27. **Hancioglu B, Swigon D, Clermont G.** 2007. A dynamical model of human immune response to influenza A virus infection. J. Theoret. Biol. **246:**70–86. http://dx.doi.org/10.1016/j.jtbi.2006.12.015.
28. **Lee HY, Topham DJ, Park SY, Hollenbaugh J, Treanor J, Mosmann TR, Jin X, Ward BM, Miao H, Holden-Wiltse J, Perelson AS, Zand M, Wu H.** 2009. Simulation and prediction of the adaptive immune response to influenza A virus infection. J. Virol. **83:**7151–7165. http://dx.doi.org/10.1128/JVI.00098-09.
29. **Saenz RA, Quinlivan M, Elton D, Macrae S, Blunden AS, Mumford JA, Daly JM, Digard P, Cullinane A, Grenfell BT, McCauley JW, Wood JLN, Gog JR.** 2010. Dynamics of influenza virus infection and pathology. J. Virol. **84:**3974–3983. http://dx.doi.org/10.1128/JVI.02078-09.
30. **Miao H, Hollenbaugh JA, Zand MS, Holden-Wiltse J, Mosmann TR, Perelson AS, Wu H, Topham DJ.** 2010. Quantifying the early immune response and adaptive immune response kinetics in mice infected with influenza A virus. J. Virol. **84:**6687–6698. http://dx.doi.org/10.1128/JVI.00266-10.
31. **Beauchemin CA, Handel A.** 2011. A review of mathematical models of influenza A infections within a host or cell culture: lessons learned and challenges ahead. BMC Public Health **11**(Suppl 1):S7. http://dx.doi.org/10.1186/1471-2458-11-S1-S7.
32. **Smith AM, Perelson AS.** 2011. Influenza A virus infection kinetics: quantitative data and models. Syst. Biol. Med. **3:**429–445. http://dx.doi.org/10.1002/wsbm.129.
33. **Smith AM, Adler FR, McAuley JL, Gutenkunst RN, Ribeiro RM, McCullers JA, Perelson AS.** 2011. Effect of 1918 PB1-F2 expression on influenza A virus infection kinetics. PLoS Comp. Biol. **7:**e1001081. http://dx.doi.org/10.1371/journal.pcbi.1001081.
34. **Canini L, Carrat F.** 2011. Population modeling of influenza A/H1N1 virus kinetics and symptom dynamics. J. Virol. **85:**2764–2770. http://dx.doi.org/10.1128/JVI.01318-10.
35. **Mitchell H, Levin D, Forrest S, Beauchemin CA, Tipper J, Knight J, Donart N, Layton RC, Pyles J, Gao P, Harrod KS, Perelson AS, Koster F.** 2011. Higher level of replication efficiency of 2009 (H1N1) pandemic influenza virus than those of seasonal and avian strains: kinetics from epithelial cell culture and computational modeling. J. Virol. **85:**1125–1135. http://dx.doi.org/10.1128/JVI.01722-10.
36. **Pawelek KA, Huynh GT, Quinlivan M, Cullinane A, Rong L, Perelson AS.** 2012. Modeling within-host dynamics of influenza virus infection including immune responses. PLoS Comp. Biol. **8:**e1002588. http://dx.doi.org/10.1371/journal.pcbi.1002588.

Downloaded from http://jvi.asm.org/ on March 31, 2014 by Helmholtz-Zentrum fuer Infektionsforschung - BIBLIOTHEK-

37. **Hernandez-Vargas EA, Meyer-Hermann M.** 2012. Innate immune system dynamics to influenza virus, p 260–265. *In* 8th IFAC Symposium on Biological and Medical Systems, vol. 8, part 1. International Federation of Automatic Control Budapest, Hungary. http://dx.doi.org/10.3182/20120829-3-HU-2029.00029.
38. **Dobrovolny HM, Reddy MB, Kamal MA, Rayner CR, Beauchemin CAA.** 2013. Assessing mathematical models of influenza infections using features of the immune response. PLoS One **8:**e57088. http://dx.doi.org/10.1371/journal.pone.0057088.
39. **Ward A.** 1997. Virulence of influenza A virus for mouse lung. Virus Genes **14:**187–194. http://dx.doi.org/10.1023/A:1007979709403.
40. **Neff-LaFord HD, Vorderstrasse BA, Lawrence B.** 2003. Fewer CTL, not enhanced NK cells, are sufficient for viral clearance from the lungs of immunocompromised mice. Cell. Immunol. **226:**54–64. http://dx.doi.org/10.1016/j.cellimm.2003.11.005.
41. **Thiebaut R, Guedj J, Jacqmin-Gadda H, Chene G, Trimoulet P, Neau D, Commenges D.** 2006. Estimation of dynamical model parameters taking into account undetectable marker values. BMC Med. Res. Methodol. **6:**38. http://dx.doi.org/10.1186/1471-2288-6-38.
42. **Storn R, Price K.** 1997. Differential evolution—a simple and efficient heuristic for global optimization over continuous spaces. J. Global Optimization **11:**341–359. http://dx.doi.org/10.1023/A:1008202821328.
43. **Xue H, Miao H, Wu H.** 2010. Sieve estimation of constant and time varying coefficients in nonlinear ordinary differential equation models by considering both numerical error and measurement error. Ann. Stat. **38:**2351–2387. http://dx.doi.org/10.1214/09-AOS784.
44. **Burham K, Anderson D.** 2002. Model selection and multimodel inference. Springer, New York, NY.
45. **Diekmann O, Heesterbeek J, Metz J.** 1990. On the definition and the computation of the basic reproduction ratio R0 in models for infectious diseases in heterogeneous populations. J. Math. Biol. **28:**365–382.
46. **Raue A, Kreutz C, Maiwald T, Bachmann J, Schilling M, Klingmller U, Timmer J.** 2009. Structural and practical identifiability analysis of partially observed dynamical models by exploiting the profile likelihood. Bioinformatics **25:**1923–1929. http://dx.doi.org/10.1093/bioinformatics/btp358.
47. **Miao H, Xia X, Perelson AS, Wu H.** 2011. On identifiability of nonlinear models and applications in viral dynamics. SIAM Rev. Soc. Ind. Appl. Math. **53:**3–39. http://dx.doi.org/10.1137/090757009.
48. **Gazit R, Gruda R, Elboim M, Arnon TI, Katz G, Achdout H, Hanna J, Qimron U, Landau G, Greenbaum E, Zakay-Rones Z, Porgador A, Mandelboim O.** 2006. Lethal influenza infection in the absence of the natural killer cell receptor gene Ncr1. Nat. Immunol. **7:**517–523. http://dx.doi.org/10.1038/ni1322.
49. **Garcıa-Sastre A, Biron CA.** 2006. Type 1 interferons and the virus-host relationship: a lesson in d'etente. Science **312:**879–882. http://dx.doi.org/10.1126/science.1125676.
50. **Price GE, Gaszewska-Mastarlarz A, Moskophidis D.** 2000. The role of alpha/beta and gamma interferons in development of immunity to influenza A virus in mice. J. Virol. **74:**3996–4003. http://dx.doi.org/10.1128/JVI.74.9.3996-4003.2000.
51. **Seo SH, Webster RG.** 2002. Tumor necrosis factor alpha exerts powerful anti-influenza virus effects in lung epithelial cells. J. Virol. **76:**1071–1076. http://dx.doi.org/10.1128/JVI.76.3.1071-1076.2002.
52. **Globerson A, Effros R.** 2000. Ageing of lymphocytes and lymphocytes in the aged. Immunol. Today **21:**515–521. http://dx.doi.org/10.1016/S0167-5699(00)01714-X.
53. **Straub RH, Cutolo M, Zietz B, Schölmerich J.** 2001. The process of aging changes the interplay of the immune, endocrine and nervous systems. Mech. Ageing Dev. **122:**1591–1611. http://dx.doi.org/10.1016/S0047-6374(01)00289-5.
54. **Pawelec G, Akbar A, Caruso C, Effros R, Grubeck-Loebenstein B, Wikby A.** 2004. Is immunosenescence infectious? Trends Immunol. **25:**406–410. http://dx.doi.org/10.1016/j.it.2004.05.006.
55. **Chen WH, Kozlovsky BF, Effros RB, Grubeck-Loebenstein B, Edelman R, Sztein MB.** 2009. Vaccination in the elderly: an immunological perspective. Trends Immunol. **30:**351–359. http://dx.doi.org/10.1016/j.it.2009.05.002.
56. **Goronzy JJ, Weyand CM.** 2013. Understanding immunosenescence to improve responses to vaccines. Nature **14:**428–436. http://dx.doi.org/10.1038/ni.2588.
57. **Zhang Y, Meyer-Hermann M, George LA, Figge MT, Khan M, Goodall M, Young SP, Reynolds A, Falciani F, Waisman A, Notley CA, Ehrenstein MR, Kosco-Vilbois M, Toellner KM.** 2013. Germinal center B cells govern their own fate via antibody feedback. J. Exp. Med. **210:**457–464. http://dx.doi.org/10.1084/jem.20120150.
58. **McGill J, Heusel JW, Legge KL.** 2009. Innate immune control and regulation of influenza virus infections. J. Leukoc. Biol. **86:**803–812. http://dx.doi.org/10.1189/jlb.0509368.
59. **Wu H, Haist V, Baumgärtner W, Schughart K.** 2010. Sustained viral load and late death in Rag2−/− mice after influenza A virus infection. Virol. J. **7:**172. http://dx.doi.org/10.1186/1743-422X-7-172.
60. **Pommerenke C, Wilk E, Srivastava B, Schulze A, Novoselova N, Geffers R, Schughart K.** 2012. Global transcriptome analysis in influenza-infected mouse lungs reveals the kinetics of innate and adaptive host immune responses. PLoS One **7:**e41169. http://dx.doi.org/10.1371/journal.pone.0041169.
61. **Davenport MP, Belz GT, Ribeiro RM.** 2009. The race between infection and immunity: how do pathogens set the pace? Trends Immunol. **30:**61–66. http://dx.doi.org/10.1016/j.it.2008.11.001.
62. **Renshaw M, Rockwell J, Engleman C, Gewirtz A, Katz J, Sambhara S.** 2002. Cutting edge: impaired Toll-like receptor expression and function in aging. J. Immunol. **169:**4697–4701.

Downloaded from http://jvi.asm.org/ on March 31, 2014 by Helmholtz-Zentrum fuer Infektionsforschung - BIBLIOTHEK-

Supplementary Material

Effects of aging on influenza virus infection dynamics

Esteban A. Hernandez-Vargas[a], Esther Wilk[c], Laetitia Canini[b], Franklin R. Toapanta[d], Sebastian C. Binder[a], Alexey Uvarovskii[a], Ted M. Ross[e], Carlos A. Guzmán[f], Alan S. Perelson[b,*], Michael Meyer-Hermann[a,g,*]

(a) Department of Systems Immunology and Braunschweig Integrated Centre of Systems Biology, Helmholtz Centre for Infection Research, Inhoffenstraße 7, Braunschweig, D-38124, Germany.

(b) Theoretical Biology and Biophysics, Los Alamos National Laboratory, Los Alamos, NM 87545, USA.

(c) Department of Infection Genetics, Helmholtz Centre for Infection Research, Inhoffenstraße 7, Braunschweig, D-38124, Germany.

(d) Center for Vaccine Development, University of Maryland, Baltimore, MD 21201, USA.

(e) Center for Vaccine Research, University of Pittsburgh, Pittsburgh, PA 15261, USA.

(f) Department of Vaccinology and Applied Microbiology, Helmholtz Centre for Infection Research, Inhoffenstraße 7, Braunschweig, D-38124, Germany.

(g) Institute for Biochemistry, Biotechnology and Bioinformatics, Technische Universität Braunschweig, 38106, Braunschweig, Germany

Received 18 December 2013 Accepted 19 January 2014
Published ahead of print 29 January 2014
Editor: A. Garcia-Sastre

Address correspondence to Alan S. Perelson, asp@lanl.gov, or Michael Meyer-Hermann, mmh@theoretical-biology.de.

A Mathematical models and Parameter values

Model	Parameter	Young mice	Aged mice
$\dot{U} = -\beta UV$	β $[10^{-6}]$	4.05	6.94
$\dot{I} = \beta UV - \delta I$	δ	1.80	9.68
$\dot{V} = pI - cV$	RMS	1.48	1.59
	AICc	50.65	62.51

Table A.1. Parameter values for model M1. The following parameters were fixed for young and aged mice: $V_0 = 25\ pfu/ml$, $p = 1\ pfu/ml \cdot d^{-1}$ and $c = 4.2\ d^{-1}$.

Model	Parameter	Young mice	Aged mice
$\dot{U} = -\beta UV$	β $[10^{-6}]$	3.06	1.64
$\dot{I} = \beta UV - \delta_T IT$	δ_T $[10^{-6}]$	2.97	7.46
$\dot{V} = pI - cV$	RMS	1.25	1.58
	AICc	30.60	57.43

Table A.2. Parameter values for model M2. The following parameters were fixed for young and aged mice: $V_0 = 25\ pfu/ml$, $p = 1\ pfu/ml \cdot d^{-1}$ and $c = 4.2\ d^{-1}$.

Model	Parameter	Young mice	Aged mice
	β $[10^{-6}]$	3.09	1.64
$\dot{U} = -\beta UV$	δ_T $[10^{-6}]$	2.97	7.46
$\dot{I} = \beta UV - \delta_T IT - \delta_K IK$	δ_K $[10^{-8}]$	1.00	1.00
$\dot{V} = pI - cV$	RMS	1.25	1.58
	AICc	32.64	62.94

Table A.3. Parameter values for model M3. The following parameters were fixed for young and aged mice: $V_0 = 25\ pfu/ml$, $p = 1\ pfu/ml \cdot d^{-1}$ and $c = 4.2\ d^{-1}$.

Model	Parameter	Young mice	Aged mice
$\dot{U} = -\beta UV$	β $[10^{-6}]$	3.00	1.56
$\dot{I} = \beta UV - \delta_K IK$	δ_K $[10^{-6}]$	3.82	26.44
$\dot{V} = pI - cV$	RMS	1.38	1.70
	AICc	42.47	72.54

Table A.4. Parameter values for model M4. The following parameters were fixed for young and aged mice: $V_0 = 25\ pfu/ml$, $p = 1\ pfu/ml \cdot d^{-1}$ and $c = 4.2\ d^{-1}$.

Model	Parameter	Young mice	Aged mice
$\dot{U} = -\beta UV - \alpha U(F_\alpha + F_\beta)$	β $[10^{-6}]$	3.53 (2.85–4.65)	2.16 (1.78–2.68) *
$\dot{I} = \beta UV - \delta_T TI$	δ_T $[10^{-6}]$	2.71 (2.40–2.96)	1.42 (1.23–1.75) *
$\dot{V} = pI - cV$	α $[10^{-3}]$	9.0 (0.10–23.31)	7.2 (4.00–11.40)
$\dot{R} = \alpha U(F_\alpha + F_\beta)$	RMS	1.22	1.36
	AICc	28.94	44.27

Table A.5. Parameter values for model M5. The 95% confidence intervals are shown in parentheses. The following parameters were fixed for young and aged mice: $V_0 = 25\ pfu/ml$, $p = 1\ pfu/ml \cdot d^{-1}$, and $c = 4.2\ d^{-1}$. Asterisks indicate statistical difference between aged and young animals. $^*p$-value<0.05.

Model	Parameter	Young mice	Aged mice
$\dot{U} = -\beta UV - \alpha UF_\gamma$	β $[10^{-6}]$	3.20	2.03
$\dot{I} = \beta UV - \delta_T TI$	δ_T $[10^{-6}]$	2.67	1.41
$\dot{V} = pI - cV$	α $[10^{-3}]$	5.70	6.20
$\dot{R} = \alpha UF_\gamma$	RMS	1.23	1.35
	AICc	30.58	43.37

Table A.6. Parameter values for model M6. The following parameters were fixed for young and aged mice: $V_0 = 25\ pfu/ml$, $p = 1\ pfu/ml \cdot d^{-1}$ and $c = 4.2\ d^{-1}$.

Model	Parameter	Young mice	Aged mice
$\dot{U} = -\beta UV - \alpha U(F_\alpha + F_\beta + F_\gamma + F_{TNF})$	β $[10^{-6}]$	3.35	2.12
$\dot{I} = \beta UV - \delta_T TI$	δ_T $[10^{-6}]$	2.68	1.41
$\dot{V} = pI - cV$	α $[10^{-3}]$	2.70	2.70
$\dot{R} = \alpha U(F_\alpha + F_\beta + F_\gamma + F_{TNF})$	RMS	1.22	1.36
	AICc	29.78	43.74

Table A.7. Parameter values for model M8. The following parameters were fixed for young and aged mice: $V_0 = 25\ pfu/ml$, $p = 1\ pfu/ml \cdot d^{-1}$ and $c = 4.2\ d^{-1}$.

B Bootstraps for the Model 5

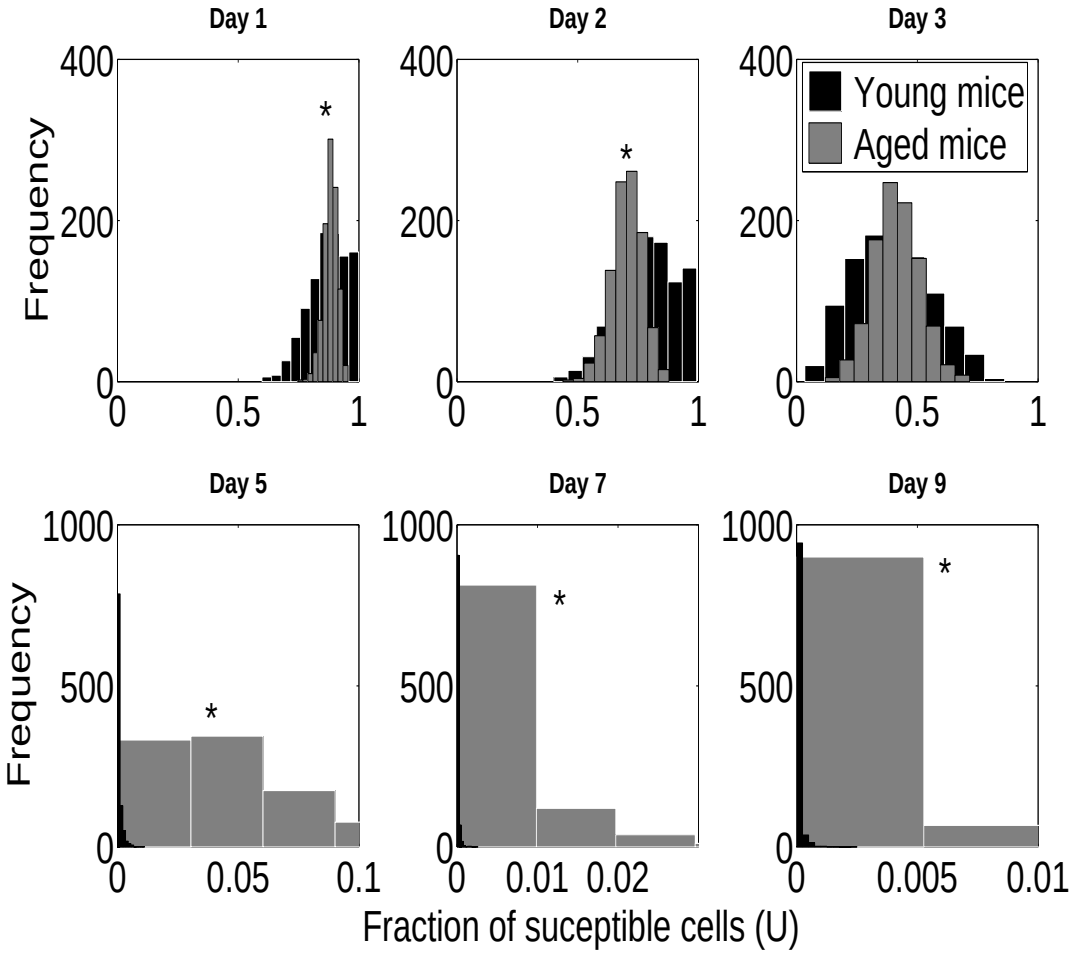

Figure B.1. Susceptible cell (U) distribution from bootstrap fits of the model M5. Asterisks indicate statistically significant differences between aged and young animals $^{*}p$-value<0.05.

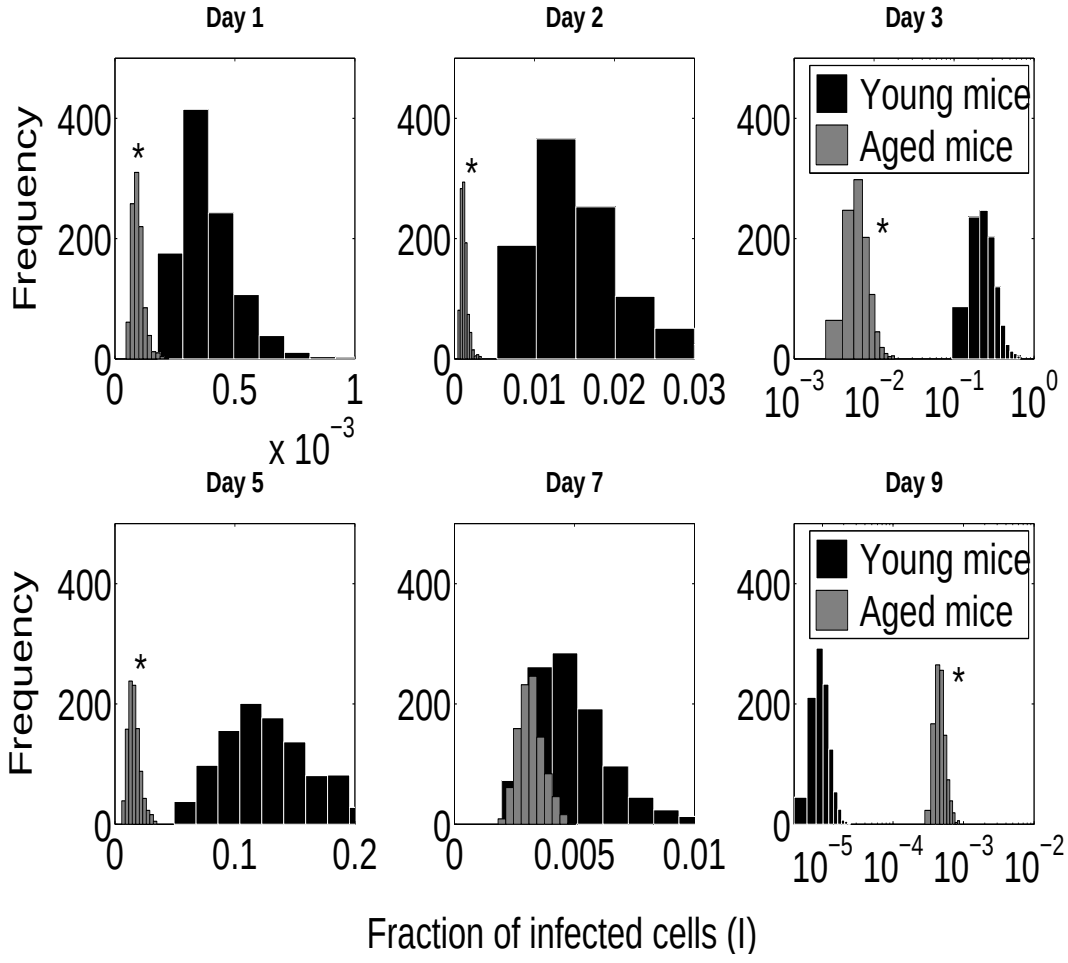

Figure B.2. Infected cell (I) distribution from bootstrap fits of the model M5. Asterisks indicate statistically significant differences between aged and young animals $^*p$-value<0.05.

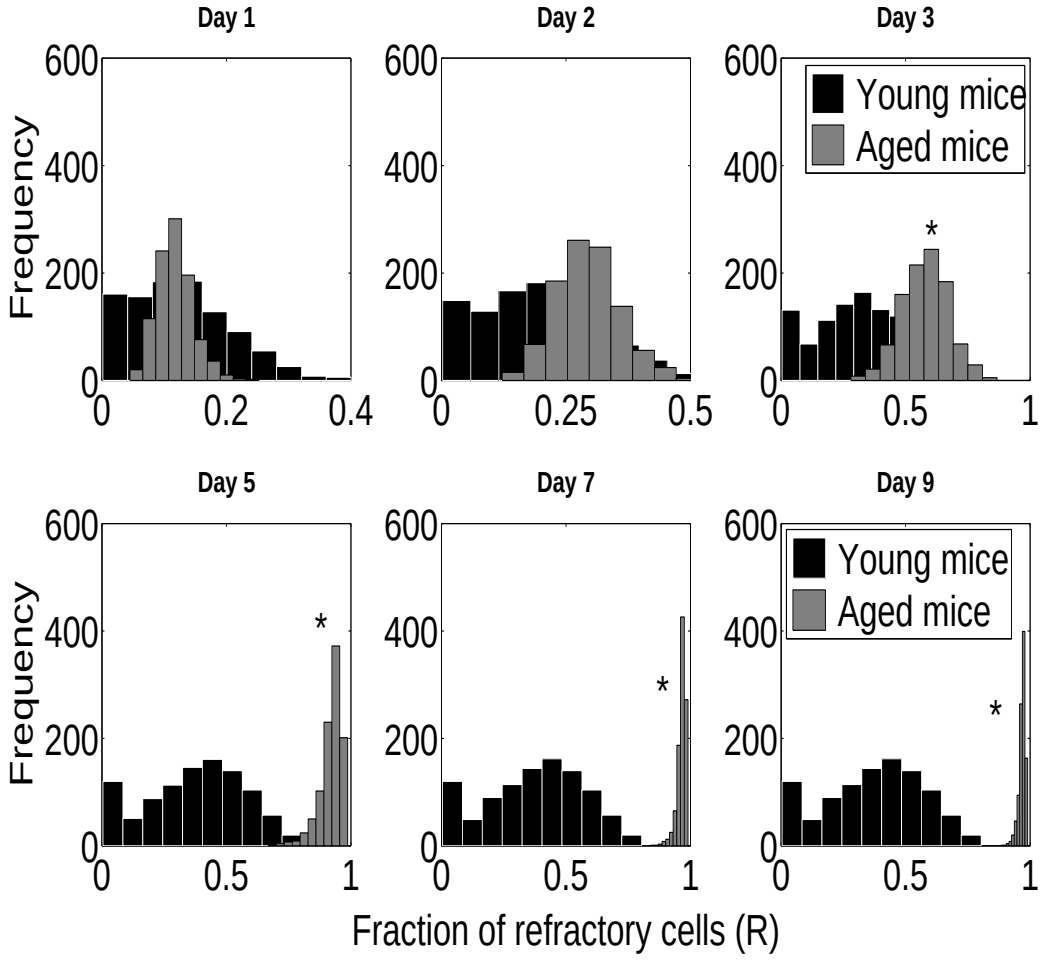

Figure B.3. Refractory cell (R) distribution from bootstrap fits of the model M5. Asterisks indicate statistically significant differences between aged and young animals $^*p$-value<0.05.

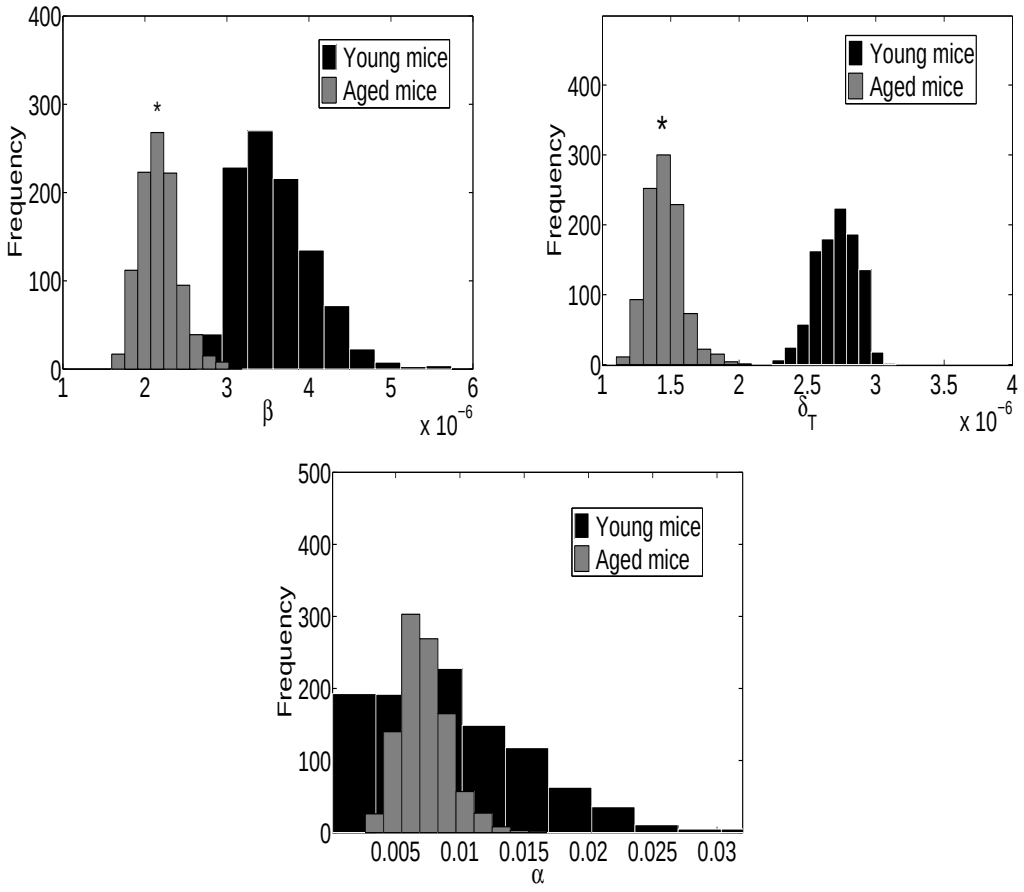

Figure B.4. Parameter distribution from bootstrap fits of the model M5. Asterisks indicate statistically significant differences between aged and young animals. $^{*}p$-value<0.05.

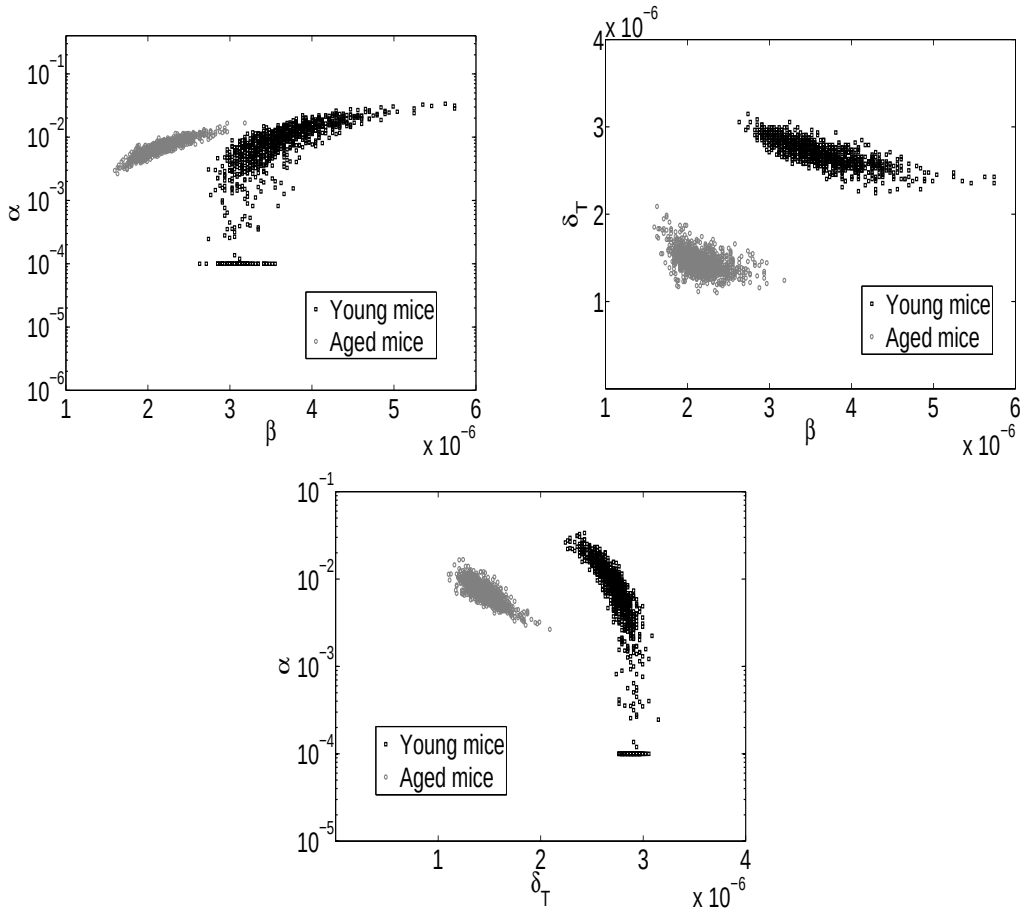

Figure B.5. Parameter ensembles from bootstrap fits of the model M5.

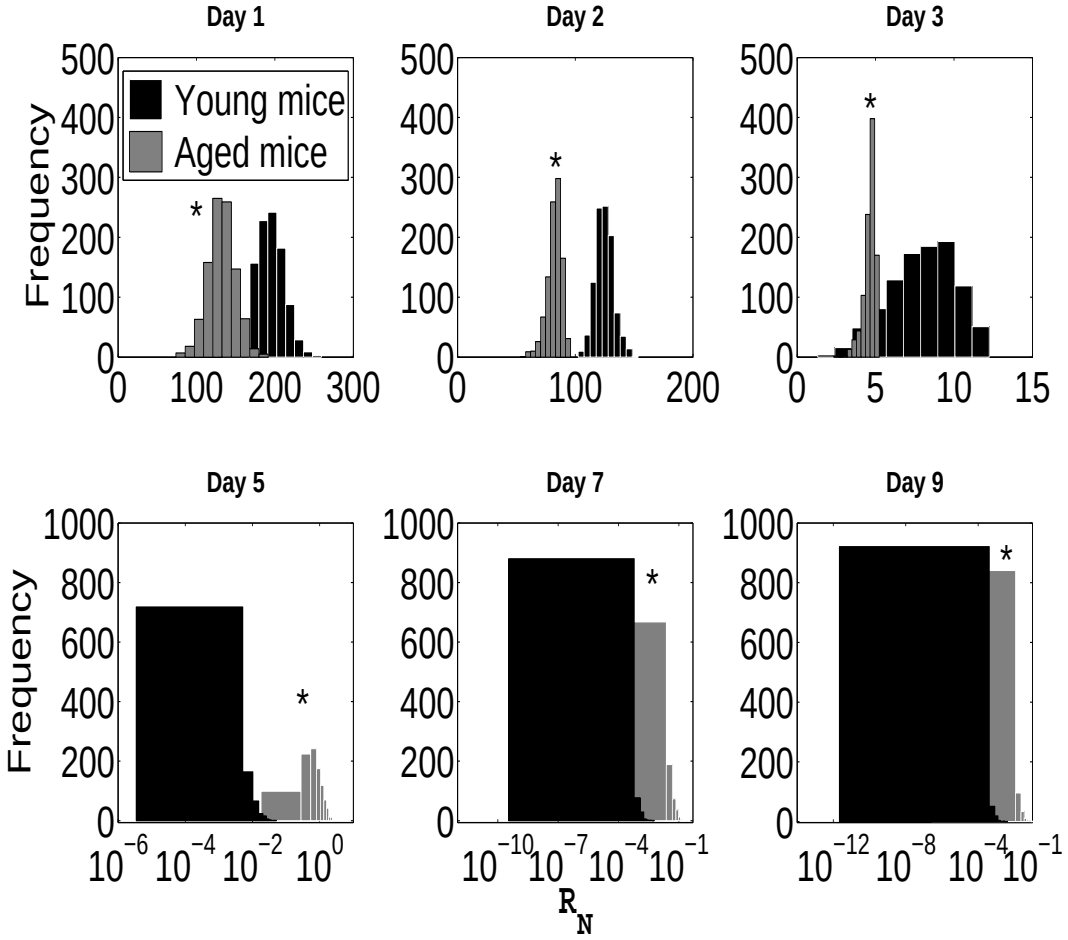

Figure B.6. Reproductive number (R_N) distribution from bootstrap fits of the model M5. Asterisks indicate statistically significant differences between aged and young animals $^*p$-value<0.05.

C Bootstraps for the Model 7

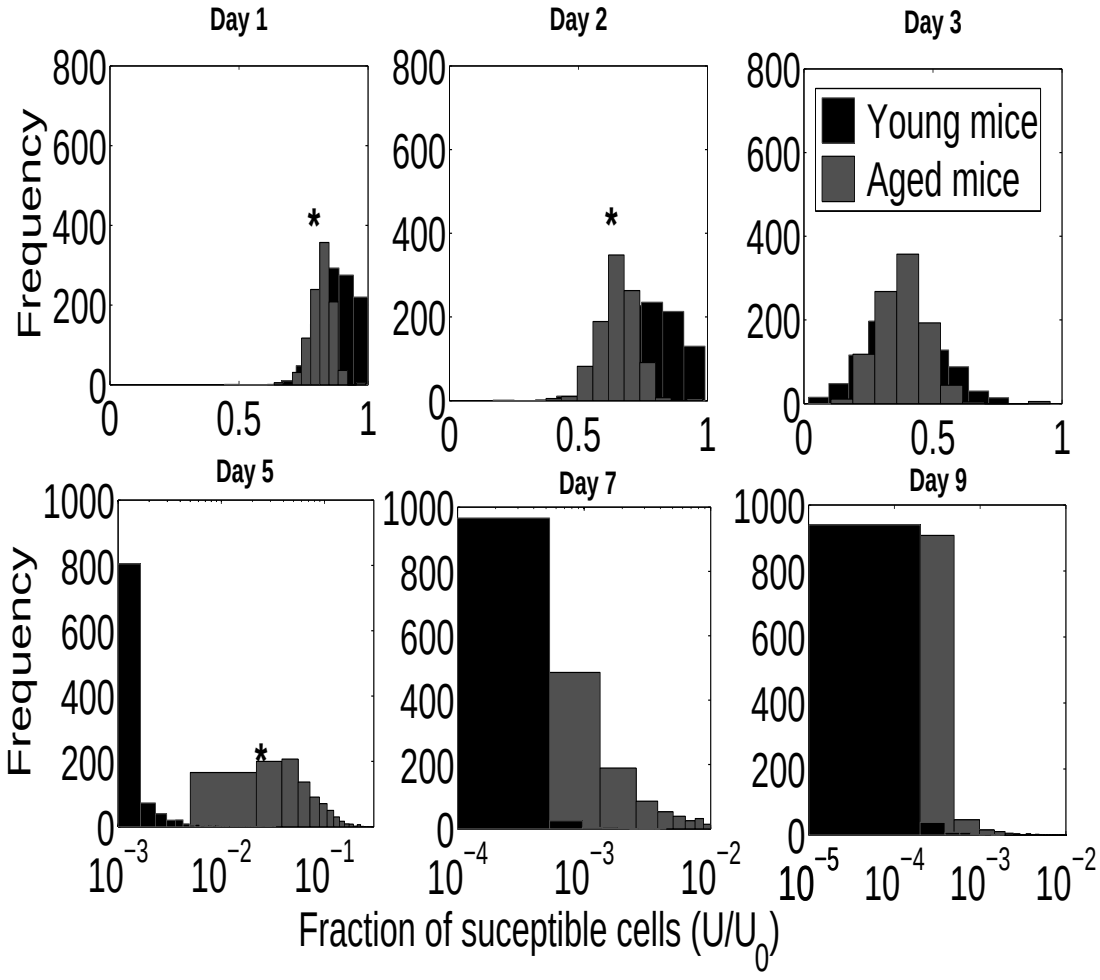

Figure C.1. Susceptible cell (U) distribution from bootstrap fits of the model M7. Asterisks indicate statistically significant differences between aged and young animals $^*p$-value<0.05.

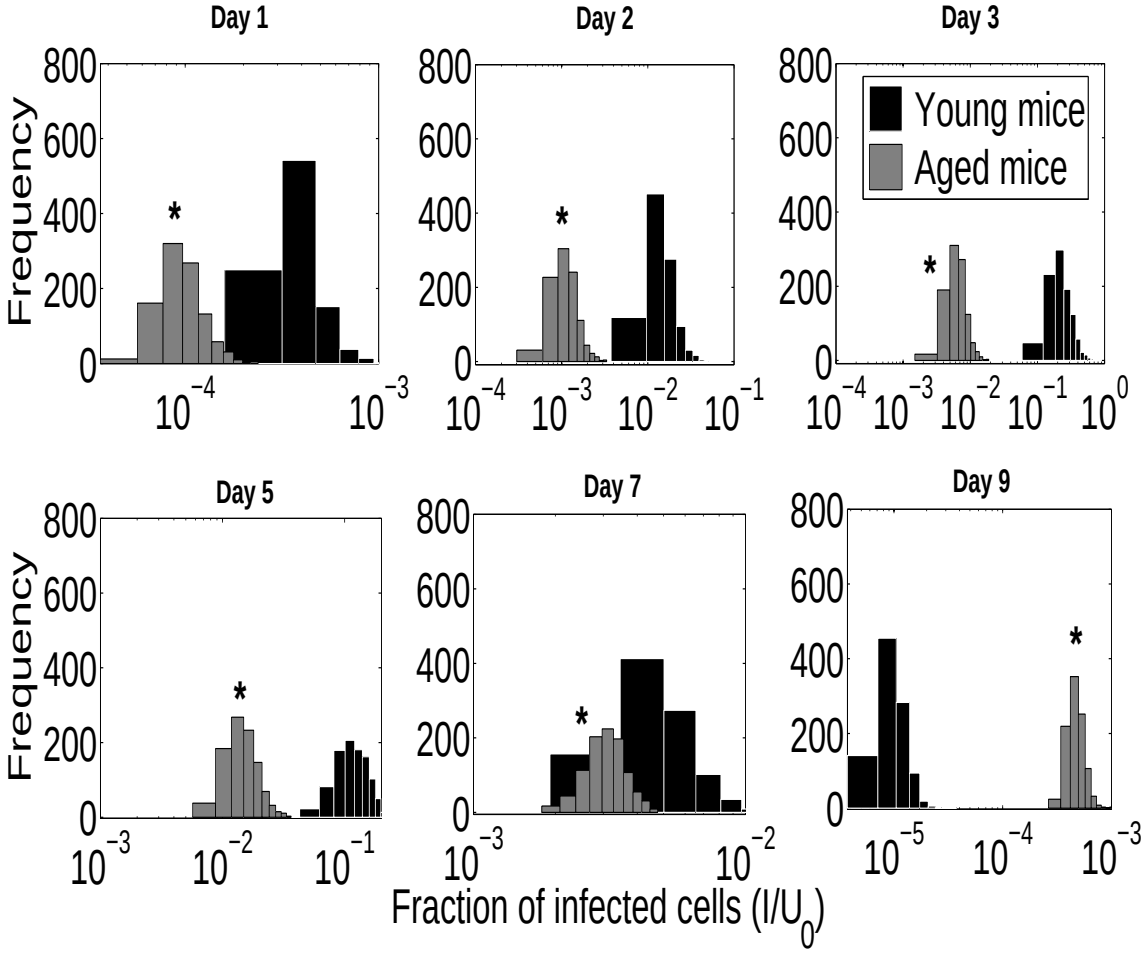

Figure C.2. Infected cell (I) distribution from bootstrap fits of the model M7. Asterisks indicate statistically significant differences between aged and young animals $^{*}p$-value<0.05.

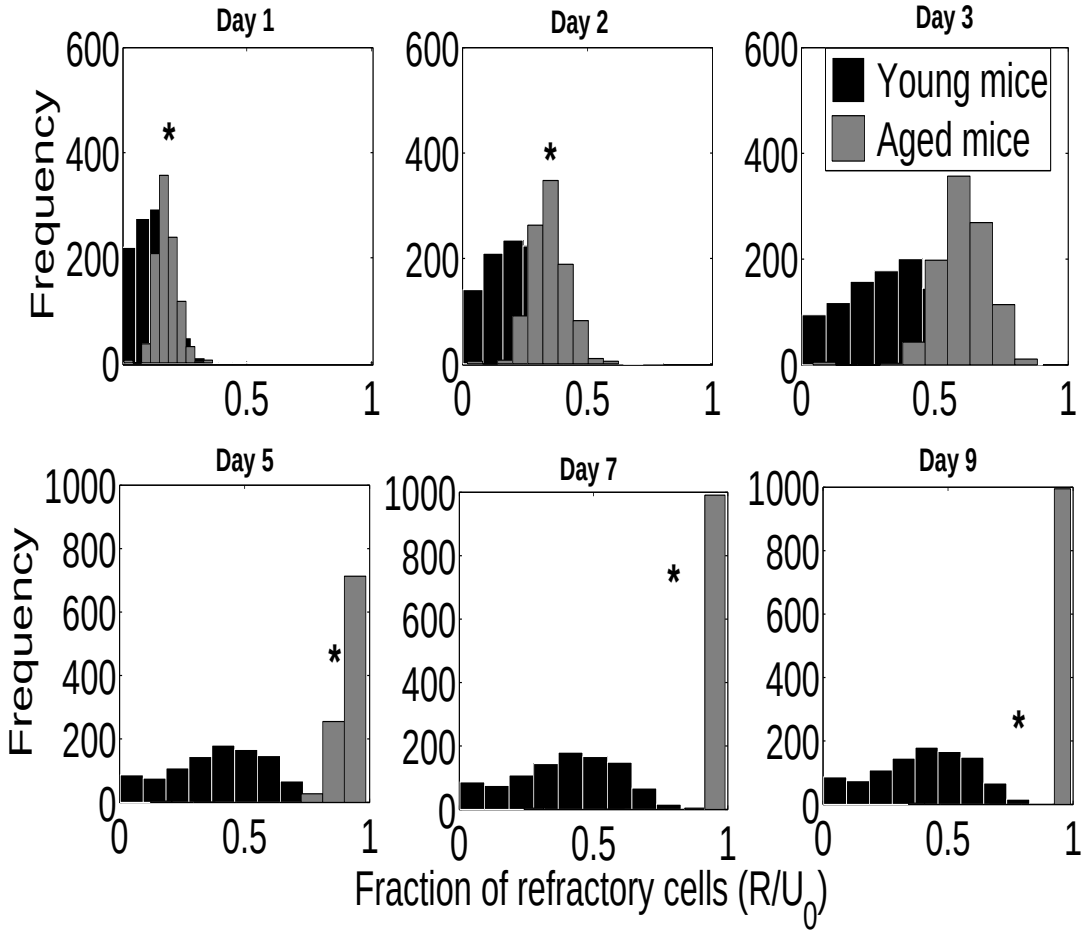

Figure C.3. Refractory cell (R) distribution from bootstrap fits of the model M7. Asterisks indicate statistically significant differences between aged and young animals $^{*}p$-value<0.05.

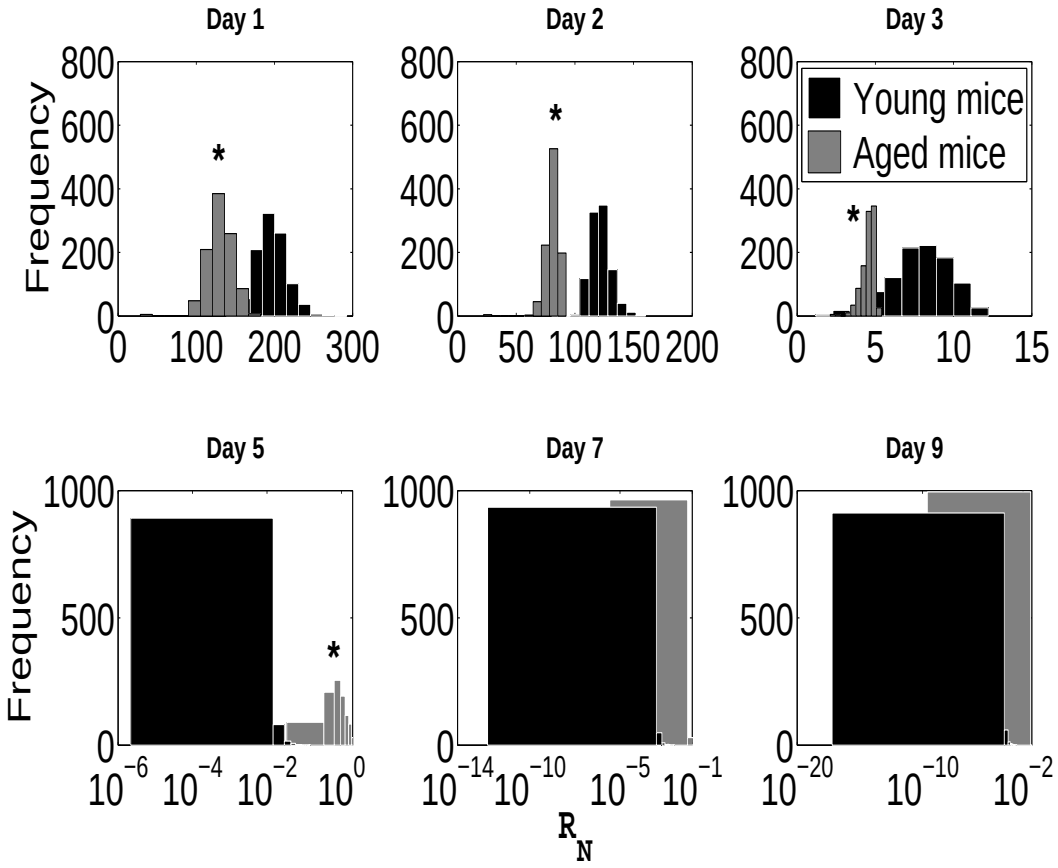

Figure C.4. Reproductive number (R_N) distribution from bootstrap fits of the model M7. Asterisks indicate statistically significant differences between aged and young animals $^*p$-value<0.05.

D Algebraic Identifiability Analysis

We investigate the algebraic identifiability of our models based on the technique presented in [1]. The idea behind this method is to identify the parameter set θ in a unique way by solving algebraic equations based only on the initial values and output measurements y_i . Therefore, a system is said to be algebraically identifiable if there exists at time t, a positive integer k, and a function ϕ such that

$$det\frac{d\phi}{d\theta} \neq 0 \tag{1}$$

and

$$\phi(\theta, y, \dot{y}, ...y^{(k)}) = 0 \tag{2}$$

holds in $[0, t]$, where det is the determinant operator, $y^{(k)}$ is the k-th derivative of y with respect to t. Equation (2) is called the identification equation, which eliminates the unobserved state variables by taking higher order derivatives. Further details of identification functions and identifiability can be found in [1–3].

Model	Identification equation
(M1)	$\phi_1 = (V^{-1}\dot{V} - \beta V)\left(\ddot{V} + \delta c V + (\delta + c)\dot{V}\right) - (\delta + c)\ddot{V} - c\delta\dot{V}$
(M2)	$\phi_2 = (V^{-1}\dot{V} - \beta V)\left(\ddot{V} + c\delta_T T V + (\delta_T T + c)\dot{V}\right) - \delta_T(\dot{T} + cT)\dot{V}$ $-(\delta_T T + c)\ddot{V} - c\delta_T \dot{T} V$
(M3)	$\phi_3 = (V^{-1}\dot{V} - \beta V)\left(\ddot{V} + c(\delta_T T + \delta_K K)V + (\delta_T T + \delta_K K + c)\dot{V}\right)$ $-\left((\delta_T \dot{T} + \delta_K \dot{K}) + c(\delta_T T + \delta_K K)\right)\dot{V} - (\delta_T T + \delta_K K + c)\ddot{V} - c(\delta_T \dot{T} + \delta_K \dot{K})V$
(M4)	$\phi_4 = (V^{-1}\dot{V} - \beta V)\left(\ddot{V} + c\delta_K K V + (\delta_K K + c)\dot{V}\right) - \delta_K(\dot{K} + cK)\dot{V}$ $-(\delta_K K + c)\ddot{V} - c\delta_K \dot{K} V$
(M5)	$\phi_5 = (V^{-1}\dot{V} - \beta V - \alpha(F_\alpha + F_\beta))\left(\ddot{V} + c\delta_T T V + (\delta_T T + c)\dot{V}\right) - \delta_T(\dot{T} + cT)\dot{V}$ $-(\delta_T T + c)\ddot{V} - c\delta_T \dot{T} V$

Table D.1. Identification function comparison using different immune strategies. The identification equation for the model M1 was obtained previously [3]. The identification equation for the models M6, M7 and M8 are equivalent to M5 equation if we substitute the term $F_\alpha + F_\beta$ by the terms F_γ, F_{TNF} and $F_\alpha + F_\beta + F_\gamma + F_{TNF}$, respectively. The full rank of the identification matrix was computed numerically.

E Practical identifiability by exploiting the profile likelihood in M7

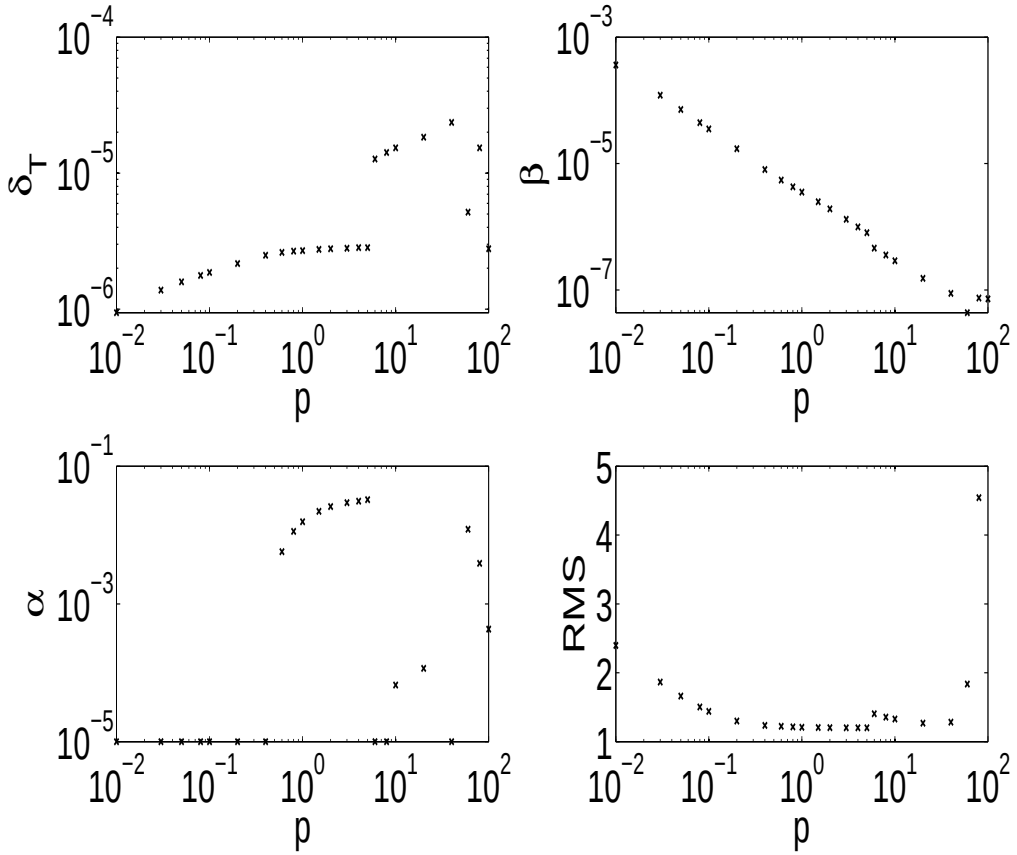

Figure E.1. Practical identifiability of parameter p for the model M7 in young mice. For each variation of the parameter p, the model M7 was refitted using the parameters β, δ_T and α.

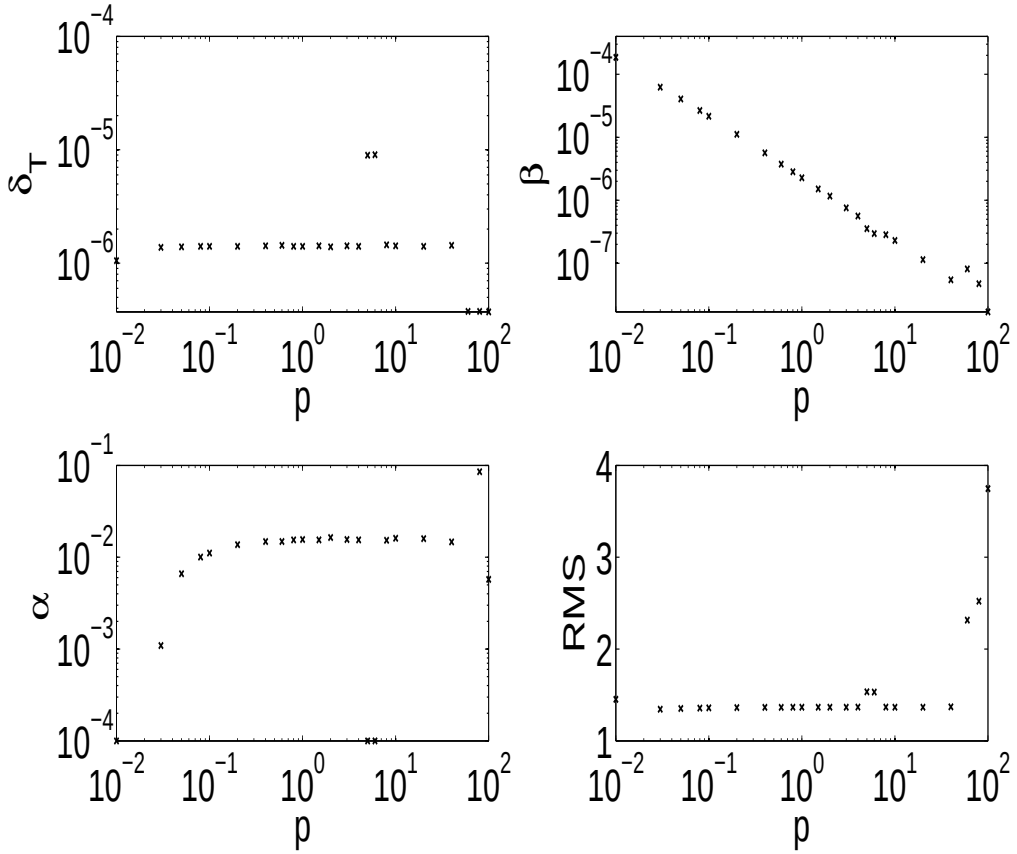

Figure E.2. Practical identifiability of parameter p for the model M7 in aged mice. For each variation of the parameter p, the model M7 was refitted using the parameters β, δ_T and α.

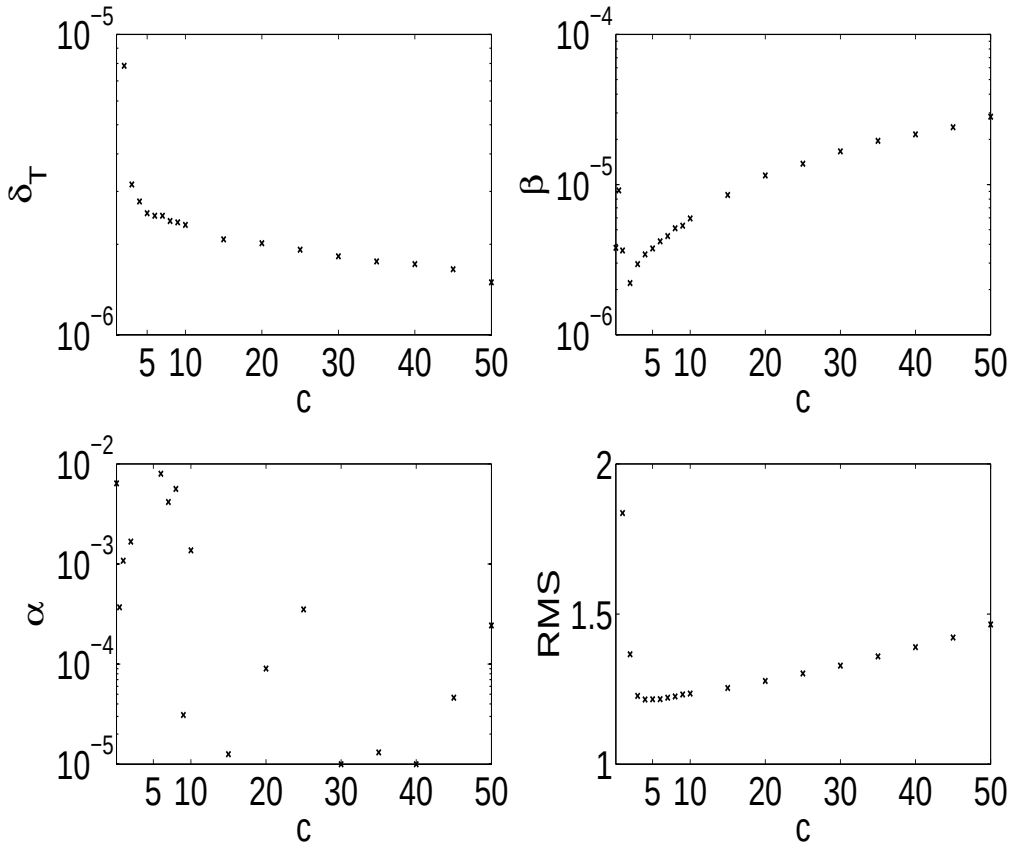

Figure E.3. Practical identifiability of parameter c for the model M7 in young mice. For each variation of the parameter c, the model M7 was refitted using the parameters β, δ_T and α.

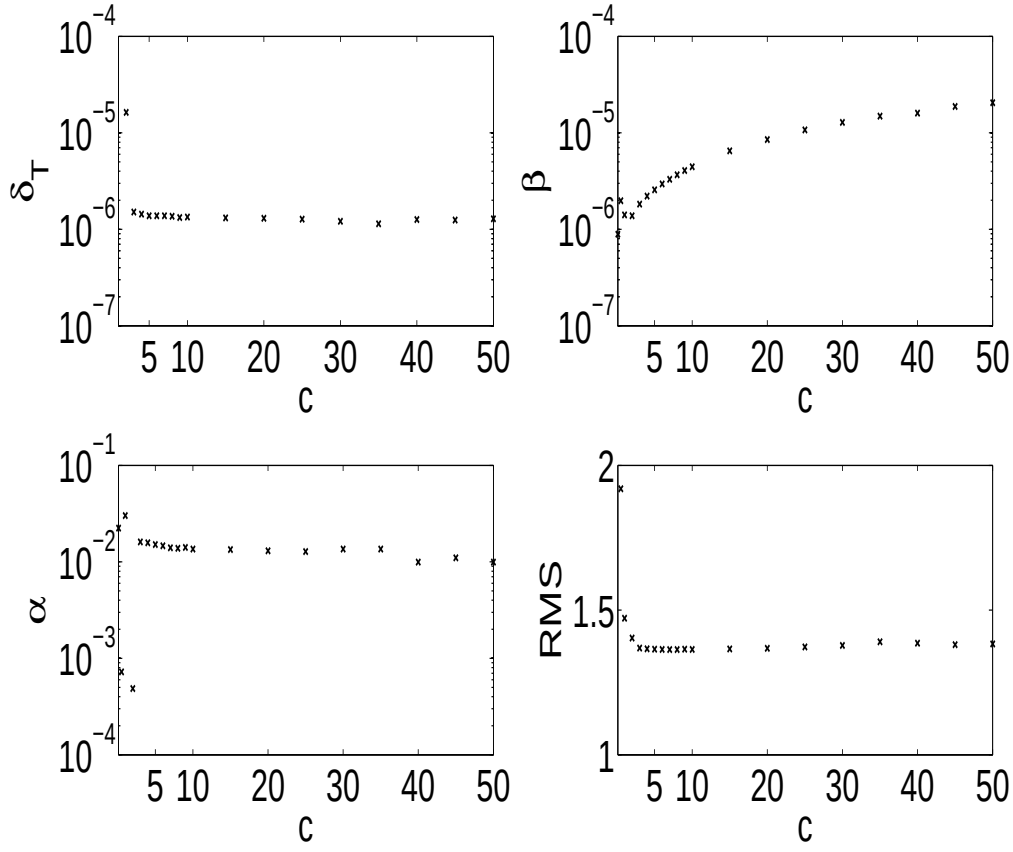

Figure E.4. Practical identifiability of parameter c for the model M7 in aged mice. For each variation of the parameter c, model M7 was refitted using the parameters β, δ_T and α.

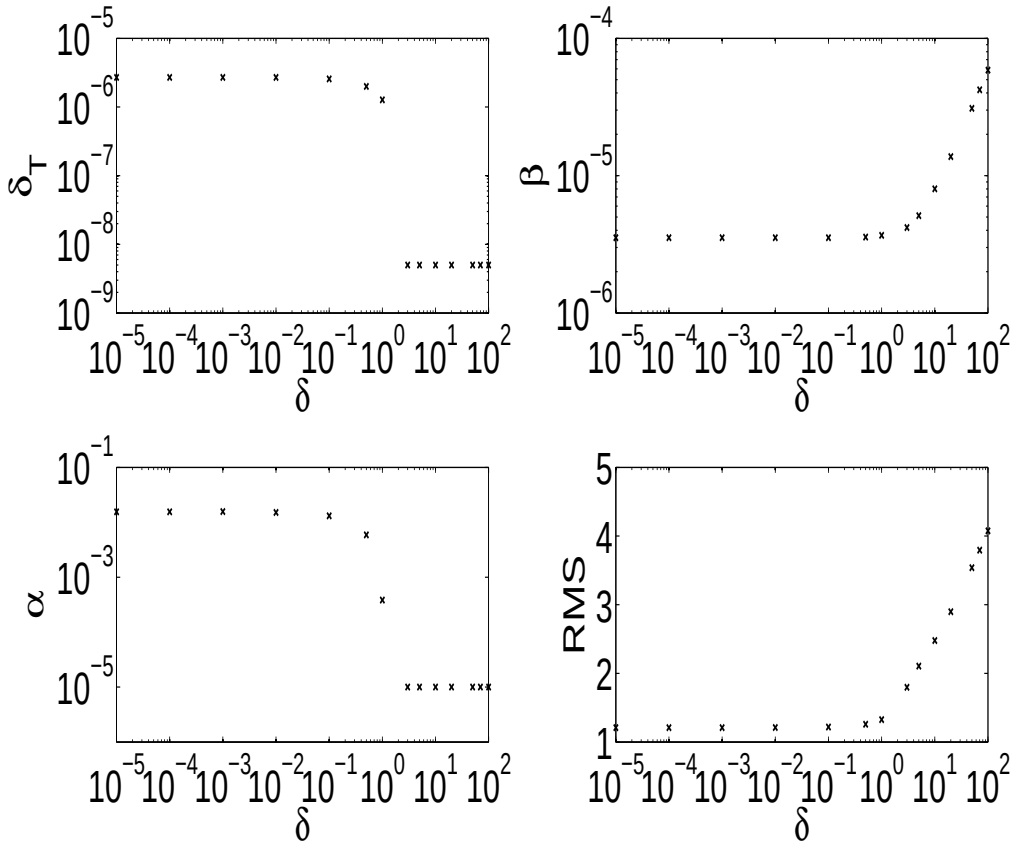

Figure E.5. Adding viral cytopathic effect to infected cells (δI) in the model M7 for young mice. For each variation of the parameter δ, model M7 was refitted using the parameters β, δ_T and α.

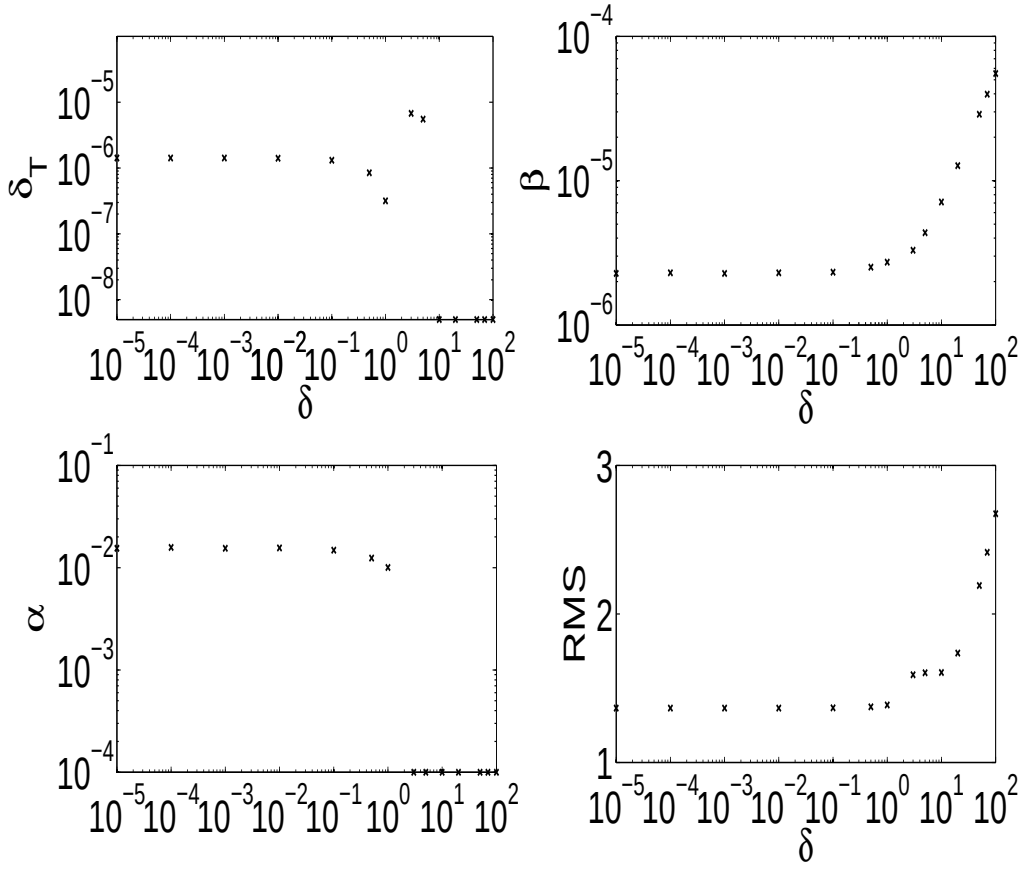

Figure E.6. Adding viral cytopathic effect to infected cells (δI) in the model M7 for aged mice. For each variation of the parameter δ, model M7 was refitted using the parameters β, δ_T and α.

References

1. **Xia, X. and C. Moog**. 2003. Identifiability of nonlinear systems with application to HIV/AIDS models. IEEE Trans Auto Cont. **48**:330–336.

2. **Wu, H., H. Zhu, H. Miao, and A. S. Perelson**. 2008. Parameter identifiability and estimation of HIV/AIDS dynamic models. Bull Math Biol. **70**:785–99.

3. **Miao, H., X. Xia, A. S. Perelson, and H. Wu**. 2011. On identifiability of nonlinear models and applications in viral dynamics. SIAM Rev. **53**:3–39.